Calibrating Networks of Low-Cost Air Quality Sensors

Priyanka deSouza[1*], Ralph Kahn[2], Tehya Stockman[3,4], William Obermann[3], Ben Crawford[5], An Wang[6], James Crooks[7], Jing Li[8], Patrick Kinney[9]

1: Department of Urban and Regional Planning, University of Colorado Denver, 80202
2: NASA Goddard Space Flight Center, Greenbelt MD
3: Denver Department of Public Health and Environment, USA
4: Department of Civil, Environmental, and Architectural Engineering, University of Colorado Boulder, Boulder, Colorado 80309, United States
5: Department of Geography and Environmental Sciences, University of Colorado Denver, 80202
6: Senseable City Lab, Massachusetts Institute of Technology, Cambridge 02139
7: Division of Biostatistics and Bioinformatics, National Jewish Health, 2930
8: Department of Geography and the Environment, University of Denver, Denver, CO, USA
9: Department of Epidemiology, University of Colorado at Denver - Anschutz Medical Campus, 129263
10: Boston University School of Public Health, Boston, MA, USA

*: priyanka.desouza@ucdenver.edu

Abstract

Ambient fine particulate matter ($PM_{2.5}$) pollution is a major health risk. Networks of low-cost sensors (LCS) are increasingly being used to understand local-scale air pollution variation. However, measurements from LCS have uncertainties that can act as a potential barrier to effective decision-making. LCS data thus need adequate calibration to obtain good quality $PM_{2.5}$ estimates. In order to develop calibration factors, one or more LCS are typically co-located with reference monitors for short- or long periods of time. A calibration model is then developed that characterizes the relationships between the raw output of the LCS and measurements from the reference monitors. This calibration model is then typically *transferred* from the co-located sensors to other sensors in the network. Calibration models tend to be evaluated based on their performance only at co-location sites. It is often implicitly assumed that the conditions at the relatively sparse co-location sites are representative of the LCS network overall, and that the calibration model developed is not overfitted to the co-location sites. Little work has explicitly evaluated how transferable calibration models developed at co-location sites are to the rest of an LCS

network, even after appropriate cross-validation. Further, few studies have evaluated the sensitivity of key LCS use-cases such as hotspot detection to the calibration model applied. Finally, there has been a dearth of research on how the duration of co-location (short-term/long-term) can impact these results. This paper attempts to fill these gaps using data from a dense network of LCS monitors in Denver deployed through the city's Love My Air program. It offers a series of transferability metrics for calibration models that can be used in other LCS networks and some suggestions as to which calibration model would be most useful for achieving different end goals.

Key words: low-cost sensors, $PM_{2.5}$, calibration, LoveMyAir

1 Introduction

Poor air quality is currently the single largest environmental risk factor to human health in the world, with ambient air pollution responsible for approximately 6.7 million premature deaths every year (State of Global Air, 2020). Having accurate air quality measurements is crucial for tracking long-term trends in air pollution levels, identifying hotspots, and for developing effective pollution management plans. The dry-mass concentration of fine particulate matter ($PM_{2.5}$), a criterion pollutant that poses more of danger to human health than other widespread pollutants (Kim et al., 2015), can vary over distances as small as ~ 10's of meters in complex urban environments (Brantley et al., 2019; deSouza et al., 2020a). Therefore, dense monitoring networks are often needed to capture relevant spatial variations. Due to their costliness, Environmental Protection Agency (EPA) air quality reference monitoring networks, the gold standard for measuring air pollutants, are sparsely positioned across the US (Apte et al., 2017; Anderson and Peng, 2012).

Low-cost sensors (LCS) (<USD $2500 as defined by the US EPA Air Sensor Toolbox) (Williams et al., 2014) have the potential to capture concentrations of PM in previously unmonitored locations and to democratize air pollution information (Castell et al., 2017; Crawford et al., 2021; Kumar et al., 2015; Morawska et al., 2018; Snyder et al., 2013; deSouza and Kinney, 2021; deSouza, 2022). However, LCS measurements have several sources of greater uncertainty than reference monitors (Bi et al., 2020; Giordano et al., 2021; Liang, 2021).

Most low-cost PM sensors rely on optical measurement techniques. Optical instruments face inherent challenges that introduce potential differences in mass estimates compared to reference methods (Barkjohn et al., 2021; Crilley et al., 2018; Giordano et al., 2021; Malings et al., 2020):

1. Optical methods do not directly measure mass concentrations; rather, they estimate mass based on calibrations that convert light scattering data to particle number and mass. LCS come with factory-supplied calibrations, but in practice must be re-calibrated in the field to ensure accuracy, due to variations in ambient particle characteristics and instrument drift.

2. High relative humidity (RH) can produce hygroscopic particle growth, leading to dry mass overestimation unless particle hydration can accurately be taken into account or the particles are dessicated by the instrument.

3. LCS are not able to detect particles with diameters below a specific size, which is determined by the wavelength of laser light within each device, and is generally in the vicinity of 0.3 μm, whereas the peak in pollution particle number size distribution is typically smaller than 0.3 μm.

4. The physical and chemical parameters describing the aerosol (particle size distribution, shape, indices of refraction, hygroscopicity, volatility etc.), that might vary significantly across different microenvironments with diverse sources, impact light scattering; this in turn affects the aerosol mass concentrations reported by these instruments.

The need for field calibration to correct LCS measurements is particularly important. This is typically done by co-locating a small number of LCS with one or a few reference monitors at a representative monitoring location or locations. The co-location could be carried out for a brief period before and/or after the actual study or may continue at a small number of sites for the duration of the study. In either case, the co-location provides data from which a calibration model is developed that relates the raw output of the LCS as closely as possible to the desired quantity as measured by the reference monitor. Thereafter, the calibration model is transferred to other LCS in the network, based upon the presumption that ongoing sampling conditions are within the same range as those at the collocation site(s) during the calibration period.

Calibration models typically correct for 1) systematic error in LCS by adjusting for bias using reference monitor measurements, and 2) the dependence of LCS measurements on environmental conditions affecting the ambient particle properties such as relative humidity (RH), temperature (T), and/or dew-point (D). Correcting for RH, T and D is carried out through either a) a physics-based approach that accounts for aerosol hygroscopic growth given particle composition using κ-Köhler's theory, or b) empirical models, such as regression and machine learning techniques. In this paper, we focus on the latter, as it is currently the most widely used (Barkjohn et al., 2021). Previous work has also shown that the two approaches yield comparable improvements in the case of $PM_{2.5}$ LCS (Malings et al., 2020).

Prior studies have used multivariate regressions, piecewise linear regressions, or higher-order polynomial models to account for RH, T and D in these calibration models (Holstius et al., 2014; Magi et al., 2020; Zusman et al., 2020). More recently, machine learning techniques such as random forests, neural networks, and gradient boosted decision trees have been used (Considine et al., 2021; Liang, 2021; Zimmerman et al., 2018).

Researchers have also started including additional covariates in their models besides what is directly measured by the LCS, such as time of day, seasonality, wind direction, and site-type, which have been shown to yield significantly improved results (Considine et al., 2021).

Past research has shown that there are several important decisions, in addition to the choice of calibration model, that need to be made during calibration and that can impact the results (Bean, 2021; Giordano et al., 2021; Hagler et al., 2018). These include a) the kind of reference air quality monitor used, b) the time-interval (e.g., hour/day) over which to average measurements used when developing the calibration model, c) how cross-validation (e.g., leave one site out/10-fold cross-validation) is carried out, and d) how long the co-location experiment takes place.

Calibration models are typically evaluated based on how well the corrected data agree with measurements from reference monitors at the corresponding co-location site. A commonly used metric is the Pearson correlation coefficient, R, which quantifies the strength of the association. However, it is a misleading indicator of sensor performance when measurements are observed close to the limit of detection of the instrument. Therefore, Root Mean Square Error (RMSE) is often included in practice. Unfortunately, neither of these metrics captures how well the calibration method developed at the co-located sites *transfers* to the rest of the network in both time and space.

If the conditions at the co-location sites (meteorological conditions, pollution source mix) for the period of co-location are the same as for the rest of the network during the total operational period, the calibration model developed at the co-location sites can be assumed to be transferable to the rest of the network. In order to ensure that the sampling conditions at the co-location site are representative of sampling conditions across the network, most researchers tend to deploy monitors in the same general sampling area as the network (Zusman et al., 2020). However, it is difficult to definitively test if the co-location site during the period of co-location is representative of conditions at all monitors in the network; ambient PM concentrations can vary on scales as small as a few meters. Furthermore, LCS are often deployed specifically in areas where the air pollution conditions are poorly understood, meaning that representativeness cannot be assessed in advance.

In order to evaluate whether calibration models are transferable in time, we test if models generated using typical short-term co-locations at specific co-location sites perform well during other time periods at all co-location sites. Where multiple co-location sites exist, one way to evaluate how transferable calibration models are in space is to leave out one or more co-location sites and test if the calibration model is transferable to the left-out sites. This method was used in recent work evaluating the feasibility of developing a US-wide calibration model for the PurpleAir low-cost sensor network (Barkjohn et al., 2021; Nilson et al., 2022).

Although these approaches are useful, co-location sites are sparse relative to other sites in the network. Even in the PurpleAir network (which is one of the densest low-cost networks in the world) there were only 39 co-location sites in 16 US states, a small fraction of the several thousand PurpleAir sites overall (Barkjohn et al., 2021). It is thus important to develop metrics to test how *sensitive* the spatial and temporal trends of pollution derived from the entire network are to the calibration model applied. Finally, a key use-case of LCS networks is to identify hotspots. It is important to also evaluate how sensitive the hotspot identified in an LCS network is to the calibration model applied.

Examining the reliability of calibration models is timely because more researchers are opting to use machine learning models. Although in most cases, such models have yielded better results than traditional linear regressions, it is important to examine if these models are overfitted to conditions at the co-location sites, even after appropriate cross-validation, and how transferable they are to the rest of the network. Indeed, because of concerns of overfitting, some researchers have explicitly eschewed employing machine learning calibration models altogether (Nilson et al., 2022). It is important to test under what circumstances such concerns might be warranted.

This paper uses a dense low-cost $PM_{2.5}$ monitoring network deployed in Denver, the "Love My Air" network deployed primarily outside the city's public schools, to evaluate the transferability of different calibration models in space and time across the network. To do so, new metrics are proposed to quantify the Love My Air network spatial and temporal trend uncertainty due to the calibration model applied. Finally, for key LCS network use-cases such as hotspot detection, tracking high pollution events and evaluating pollution trends at a high temporal resolution, the sensitivity of the results to the choice of calibration model is evaluated. The methodologies and metrics proposed in this paper can be applied to other low-cost sensor networks, with the understanding that the actual results will vary with study region.

2 Data and Methods

2.1 Data Sources

Between Jan 1 and Sep 30, 2021, Denver's Love My Air sensor network collected minute-level data from 24 low-cost sensors deployed across the city outside of public schools and at 5 federal equivalent method (FEM) reference monitor locations (**Figure 1**). The Love My Air sensors are Canary-S models equipped with a Plantower 5003, made by Lunar Outpost Inc. The Canary-S sensors detect $PM_{2.5}$, T, and RH, and upload minute-resolution measurements to an online platform via cellular data network.

We found that RH and T reported by the Love My Air sensors were well correlated with that reported by the reference monitoring stations. We used the Love My Air LCS T and

RH measurements in our calibration models as they most closely represent the conditions experienced by the sensors.

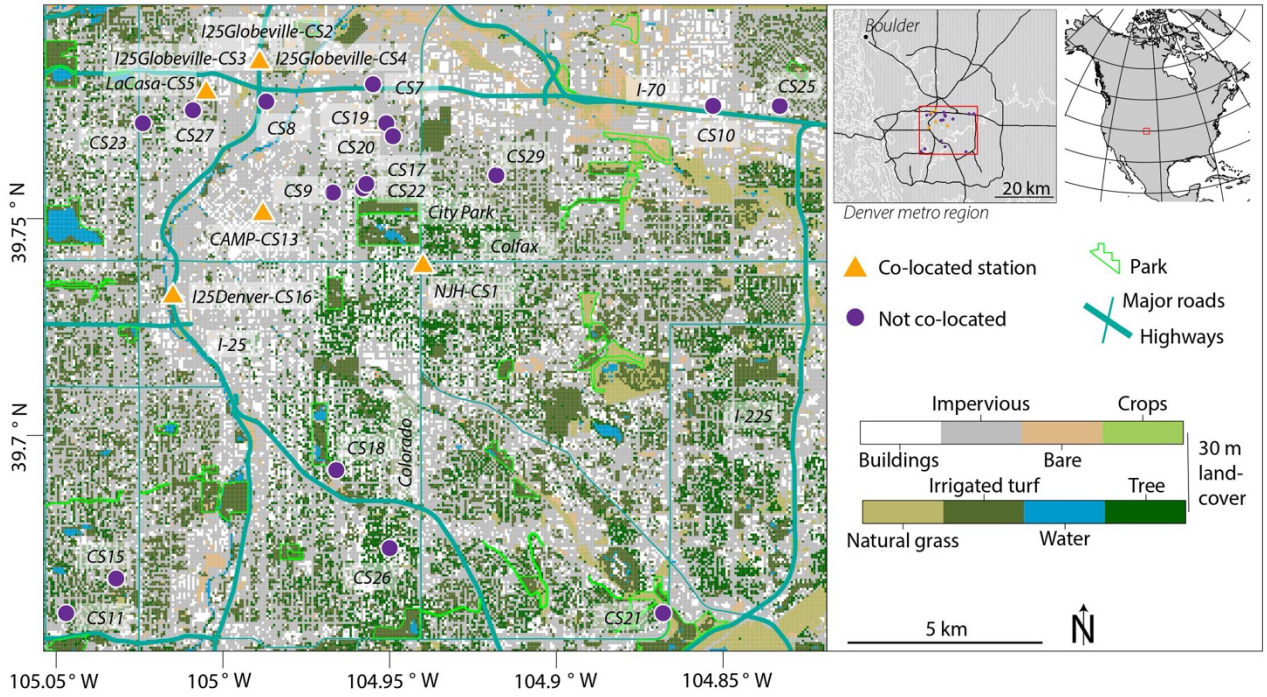

***Figure 1**: Locations of all 24 Love My Air sensors. Sensors displayed with an orange triangle indicate that they were co-located with a reference monitor. The labels of the co-located sensors include the name of the reference monitor with which they were co-located after a hyphen.*

2.1.1 Data cleaning protocol for measurements from the Love My Air network

A summary of the data cleaning and data preparation steps carried out on the Love My Air data from the entire network are listed below:

1) Removed data for time-steps where key variables: $PM_{2.5}$, T and RH measurements were missing
2) Removed unrealistic RH and T values (RH < 0 and T ≤ -30^{0}C)
3) Removed $PM_{2.5}$ values above 1,500 µg/m^3 (outside the operational range of the Plantower sensors used) from the Canary-S sensors (Considine et al., 2021)
4) We were left with 8,809,340 minute-level measurements and then calculated hourly-average $PM_{2.5}$, T, and RH measurements for each sensor. We had a total of 147,101 hourly-averaged measurements
5) From inspection, one of the monitors, CS13, worked intermittently in Jan and Feb, before resuming continuous measurement in March (**Figure S1** *in Supplementary Information*). When CS13 worked intermittently, large spikes in the measurements were observed, likely due to power surges. We thus retained measurements taken after March 1, 2021 for this monitor. The total number of hourly measurements was thus reduced to 146,583.

Love My Air sensors (indicated by Sensor ID) were co-located with FEM reference monitors from which we obtained high quality hourly $PM_{2.5}$ measurements at (**Table 1**):

1) La Casa (Sensor ID: CS5)
2) CAMP (Sensor ID: CS13)
3) I25 Globeville (Sensor ID: CS2, CS3, CS4)
4) I25 Denver (Sensor ID: CS16)
5) NJH (Sensor ID: CS1) for the entire period of the experiment

2.1.2 Data preparation steps for preparing a training dataset used to develop the various calibration models

A summary of the data preparation steps for preparing a training dataset used to develop the various calibration models are described below:

1) We joined hourly averages from each of the seven co-located Love My Air monitors with the corresponding FEM monitor. We had a total of 35,593 co-located hourly measurements for which we had data for both the Love My Air sensor and the corresponding reference monitor.
   Figure S2 displays time-series plots of $PM_{2.5}$ from all co-located Love My Air sensors. **Figure S3** displays time-series plots of $PM_{2.5}$ from the corresponding reference monitors.
2) The three Love My Air sensors co-located at the I25 Globeville sites (CS2, CS3, CS4) agreed well with each other (correlation = 0.98) (**Figures S4** and **Figure S5**). To ensure that our co-located dataset was well balanced across sites, we only retained measurements from CS2 at the I25 Globeville site. We were left with a total of 27,338 co-located hourly measurements that we used to develop a calibration model. **Figure S6** displays the time-series plots of $PM_{2.5}$ from all other Love My Air sensors in the network.

Reference monitors at La Casa, CAMP, I25 Globeville and I25 Denver, also reported minute-level $PM_{2.5}$ concentrations between April 23 11:16 and Sep 30, 22:49. We also joined minute-level Love My Air $PM_{2.5}$ concentrations with minute-level reference data at these sites. We had a total of 1,062,141 co-located minute-level measurements during this time period. As with the hourly-averaged data, we only retained data from one of the Love My Air sensors at the I25 Globeville site and were thus left with 815,608 minute-level measurements from one LCS at each of the four co-location sites.

Table S1 has information on the minute-level co-located measurements. The data at the minute-level displays more variation and peaks in $PM_{2.5}$ concentrations than the hourly-averaged measurements (**Figure S7)**, likely due to the impact of passing sources. It is also important to mention that minute-level reference data may have some additional uncertainties introduced due to instrument error given the finer time resolution. We will

use the minute-level data in supplementary analyses, only. Thus, unless explicitly referenced, we will be reporting results from hourly-averaged measurements.

2.1.3 Deriving additional covariates

We derived dew-point (D) from T and RH reported by the Love My Air sensors using the *weathermetrics* package in the programming language R (Anderson and Peng, 2012), as D has been shown to be a good proxy of particle hygroscopic growth in previous research (Barkjohn et al., 2021; Clements et al., 2017; Malings et al., 2020). Some previous work has also used a nonlinear correction for RH in the form of $RH^2/(1\text{-}RH)$, that we also calculated for this study (Barkjohn et al., 2021).

We extracted hour, weekend, and month variables from the Canary-S sensors and converted hour and month into cyclic values to capture periodicities in the data by taking the cosine and sine of hour*$2\pi/24$ and month*$2\pi/12$, which we designate as cos_time, sin_time, cos_month and sin_month, respectively. Sinusoidal corrections for seasonality have been shown to improve accuracy of $PM_{2.5}$ measurements in machine learning models (Considine et al., 2021).

Table 1*: Site location of each Love My Air sensor, as well as summary statistics of hourly measurements from each sensor*

					$PM_{2.5}$ (µg/m^3)			Temperature (^{0}C)	RH (%)	Dewpoint (^{0}C)
Sensor ID	**Co-location Information**	**Latitude**	**Longitude**	**Hours operational**	**Mean**	**Median**	**Min-Max**	**Mean**	**Mean**	**Mean**
CS1	Co-located at NJH	39.739	-104.940	5,478	13	8	0 - 121	14.9	57.4	4.4
CS2	Co-located at I25 Globeville	39.786	-104.989	5,818	14	9	0 - 142	16.4	63.6	7.6
CS3	Co-located at I25 Globeville	39.786	-104.989	2,490	18	13	0 - 159	9.3	62.5	0.1
CS4	Co-located at I25 Globeville	39.786	-104.989	5,765	12	8	0 - 137	15.8	67.6	8.0
CS5	Co-located at La Casa	39.779	-105.005	5,761	12	8	0 - 129	13.4	69.6	6.0
CS7	-	39.781	-104.955	6,540	13	8	0 - 136	16.5	55.6	5.0
CS8	-	39.777	-104.987	6,282	13	8	0 - 133	17.3	38.3	0.0
CS9	-	39.756	-104.967	6,552	12	8	0 - 115	15.3	62.8	6.1
CS10	-	39.776	-104.853	6,552	12	7	0 - 142	17.9	32.6	-2.4
CS11	-	39.659	-105.047	6,548	12	7	0 - 127	15.0	58.2	4.5
CS13	Co-located at CAMP	39.751	-104.988	4,449	13	8	0 - 115	21.9	54.7	10.2
CS15	-	39.667	-105.032	6,552	10	6	0 - 106	17.0	34.6	-1.5
CS16	Co-located at I25 Denver	39.732	-105.015	5,832	12	9	0 - 100	17.4	33.6	-2.2

CS17	-	39.757	-104.958	6,527	12	7	0 - 149	17.1	35.1	-1.3
CS18	-	39.692	-104.966	6,552	12	7	0 - 115	16.9	36.3	-1.0
CS19	-	39.772	-104.951	1,749	11	5	0 - 66	3.4	40.0	-11.1
CS20	-	39.769	-104.949	6,551	10	6	0 - 105	17.9	34.2	-1.2
CS21	-	39.659	-104.868	6,551	12	6	0 - 129	15.2	39.2	-1.2
CS22	-	39.758	-104.957	6,551	12	7	0 - 118	17.5	35.4	-0.9
CS23	-	39.772	-105.024	6,552	14	9	0 - 139	16.5	34.6	-2.0
CS25	-	39.776	-104.833	6,551	12	7	0 - 135	16.2	35.8	-1.8
CS26	-	39.674	-104.950	6,552	12	7	0 - 115	15.9	36.9	-1.2
CS27	-	39.775	-105.009	6,552	12	7	0 - 115	16.4	35.6	-1.4
CS29	-	39.760	-104.918	6,552	11	7	0 - 114	15.7	37.5	-1.2

2.2 Defining the Calibration Models Used

The goal of the calibration model is to predict, as accurately as possible, the 'true' $PM_{2.5}$ concentrations given the concentrations reported by the Love My Air sensors. At the co-located sites, the FEM $PM_{2.5}$ measurements, which we take to be the "true" $PM_{2.5}$ concentrations, are the dependent variable in the models.

We evaluated 21 increasingly complex models that included T, RH, D as well as metrics that captured the time-varying patterns of $PM_{2.5}$ to correct the Love My Air $PM_{2.5}$ measurements (**Tables 2** and **3**).

Sixteen models were multivariate regression models that were used in a recent paper (Barkjohn et al., 2021) to calibrate another network of low-cost sensors: the PurpleAir, that rely on the same $PM_{2.5}$ sensor (Plantower) as the Canary-S sensors in the current study. As T, RH, and D are not independent (**Figure S8**), the 16 linear regression models include adding the meteorological conditions considered as interaction terms, instead of additive terms. The remaining five calibration models relied on machine learning techniques.

Machine learning models can capture more complex nonlinear effects (for instance, unknown relationships between additional spatial and temporal variables). We opted to use the following machine learning techniques: Random Forest (RF), Neural Network (NN), Gradient Boosting (GB), SuperLearner (SL) that have been widely used in calibrating LCS. A description of each technique is described in detail in **section S1** in *Supplementary Information*. All machine learning models were run using the *caret* package in R (Kuhn, 2015).

We used both Leave-One-Site-Out (LOSO) (**Table 2**) and Leave-Out-By-Date, where we left out a 3-weeks period of data at a time at all sites (LOBD) (**Table 3**) cross-validation (CV) methods to avoid overfitting in the machine learning models. For more details on the cross-validation methods used to avoid overfitting in the machine learning models refer to **section S2** in *Supplementary Information*.

2.2.1 Corrections generated using different co-location time periods (long-term, on-the-fly, short-term)

As described earlier, co-location studies in the LCS literature have been conducted over different time periods. Some studies co-locate one or more LCS for brief periods of time before or after an experiment, whereas others co-locate a few LCS for the entire duration of the experiment. These studies apply calibration models generated using the co-located data to measurements made by the entire network over the entire duration of the experiment. We attempt to replicate these study designs in our experiment to evaluate the transferability of calibration models across time by generating four different corrections:

(C1) *Entire data set correction*: The 21 calibration models were developed using data at all co-location sites for the entire period of co-location.
(C2) *On the fly correction:* The 21 calibration models to correct a measurement during a given week were developed using data across all co-located sites for the same week of the measurement.
(C3) *2-week winter correction:* The 21 calibration models were developed using co-located data collected for a brief period (2 weeks) at the beginning of the study (Jan 1 - Jan 14, 2021). They were then applied to measurements from the network during the rest of the period of operation.
(C4) *2-week winter + 2-week spring:* The 21 calibration models were developed using co-located data collected for two 2-week periods in different seasons (Jan 1 - Jan 14, 2021 and May 1 - May 14, 2021). They were then applied to measurements from the network during the rest of the period of operation.

Although models developed using co-located data over the entire time period (C1) tend to be more accurate over the entire spatiotemporal data set, it is inefficient to re-run large models frequently (incorporating new data). On-the-fly corrections (such as C2) can help characterize short-term variation in air pollution and sensor characteristics. The duration of calibration is a key question that remains unanswered (Liang, 2021). We opted to test corrections C3 and C4 as many low-cost sensor networks rely on developing calibration models based on relatively short co-location periods (deSouza et al., 2020b; West et al., 2020; Singh et al., 2021). Each of the 21 calibration models considered was tested under four potential correction schemes (C1, C2, C3 and C4).

For C1, the five machine-learning models were trained using two CV approaches: LOSO and LOBD, separately. For C2, C3 and C4 only LOSO was conducted, as model

application is already being performed on a different time period from the training (for more details refer to **section S2**).

Overall, we test 89 calibration models (21 (C1, CV=LOSO) + 5 (C1, CV=LOBD) + 21 × 3 (C2, C3, C4) = 89) listed in **Tables 2** and **3**.

2.3 Evaluating the calibration models developed under the four different correction schemes

Uncorrected Love My Air measurements tend to be biased upwards from the corresponding reference $PM_{2.5}$ levels by an average of ~12% (**Figure S9**). We first evaluate:

1) Were meteorological conditions at the co-location sites representative of network operating conditions?
2) How well do different calibration models perform when using the traditional method of model evaluation at co-location sites, during the period of co-location?

We then evaluate transferability of the calibration models in time and space by evaluating:

1) How well do calibration models developed during short-term co-locations (corrections: C3 and C4) perform when transferred to long-term network measurements?
2) How well do calibration models developed at a small number of co-locations sites transfer in space to other sites, even after appropriate cross-validation to prevent overfitting?
3) Different metrics to quantify the uncertainty in spatial and temporal trends in $PM_{2.5}$ reported by the LCS network to the calibration model applied.

Finally, we evaluate the impact of the choice of calibration model on key LCS network use-cases, such as hotspot detection, or detection of the most-polluted site. In supplementary analyses, we also evaluate how much the calibration model impacts the following additional use-cases:

1) LCS are increasingly used to evaluate pollution trends on increasingly short timescales. We evaluated how well calibration models developed using hourly aggregated data to minute-level LCS measurements
2) LCS have been deployed to track smoke from fires. We evaluate how well different calibration models perform at high $PM_{2.5}$ concentrations.

2.3.1 Evaluating the representativeness of meteorological conditions at the co-location sites of the entire network

LCS measurements are impacted by T and RH. We thus, first evaluated if meteorological conditions (T and RH) at the co-location sites during time-periods used to construct the calibration models were representative of conditions of operation for the rest of the network by comparing distributions of these parameters across sites (**Figure 2**).

2.3.2 Traditional Evaluation of the different Calibration Models

We evaluated the performance of the calibration models for the time period of co-location in our sample using: R (Pearson correlation coefficient), and RMSE (**Tables 2** and **3**).

2.3.3 Evaluating transferability of short-term calibrations developed to the entire period of operation of the network

We evaluated calibration models using corrections C3 and C4 only for the time-period over which the calibration models were developed, which was Jan 1 - Jan 14, 2021, for C3 and Jan 1 - Jan 14, 2021, and May 1 - May 14, 2021, for C4 (**Table S2**) and compared the performance with applying these models to the entire time period of the network (**Table 2**).

2.3.4 Evaluating whether the calibration models are overfitted to the co-location sites even after appropriate cross-validation

To evaluate how transferable the calibration technique developed at the co-located sites was to the rest of the network, even after conducting LOSO CV, we left out each of the five co-located sites in turn and using data from the remaining sites ran the models proposed in **Tables 2** and **3**. We then applied the models generated to the left-out site. We report the distribution of RMSE from each calibration model considered at the left-out sites using box-plots (**Figure 3**). For correction C1, we also left out a three-week period of data at a time and generated the calibration models based on the data from the remaining time periods at each site. For the machine learning models (Models 17 – 21), we used CV = LOBD. We plotted the distribution of RMSE from each model considered for the left-out three week period (**Figure 3**).

We statistically compared the errors in predictions on each test dataset with errors in predictions from using all sites in our main analysis. Such an approach is useful to understand how well the proposed correction can transfer to other areas in the Denver region. To compare statistical differences between errors, we used t-tests if the distribution of errors were normally distributed (as determined by a Shapiro–Wilk test), and Wilcoxon signed rank tests, if not, using a significance value of 0.05 (**Section 3.1.4**).

We have only five co-location sites in the network. Although evaluating the transferability among these sites is useful, as we know the true $PM_{2.5}$ concentrations at these sites, we also evaluated the transferability of these models in the larger network by predicting $PM_{2.5}$ concentrations using the models proposed in **Tables 2** and **3** at each of the 24 sites in the Love My Air network. For each site, we display time series plots of corrected $PM_{2.5}$ measurements in order to visually compare the ensemble of corrected values at each site (**Figure 3**).

2.3.5 Evaluating sensitivity of the spatial and temporal trends of the low-cost sensor network to the method of calibration

We evaluate the spatial and temporal trends in the $PM_{2.5}$ concentrations corrected using the 89 different calibration models using similar methods to that described in (Jin et al., 2019; deSouza et al., 2022) by calculating:

(1) The spatial root mean square difference (RMSD) (**Figure 5**) between any two corrected exposures at the same site: $SRMSD_{h,d} = \sqrt{\frac{1}{N}\sum_{i=1}^{N} (Conc_{hi} - Conc_{di})^2}$, where $Conc_{hi}$ and $Conc_{di}$ are Jan 1- Sep 30, 2021 averaged $PM_{2.5}$ concentrations estimated from correction *h* and *d* for site *i*. *N* is the total number of sites.

(2) The temporal RMSD (**Figure 6**) between pairs of exposures: $TRMSD_{h,d} = \sqrt{\frac{1}{M}\sum_{t=1}^{M} (Conc_{ht} - Conc_{dt})^2}$, where $Conc_{ht}$ and $Conc_{dt}$ are hourly corrected $PM_{2.5}$ concentrations averaged over all operational Love My Air sites estimated from correction *h* and *d* for time *t*. *M* is the total number of hours of operation of the network.

(3) The spatial Pearson correlation coefficient (**Figure 7**): $R_S = \frac{\sum_{i=1}^{N} (Conc_{hi} - \overline{Conc_h})(Conc_{di} - \overline{Conc_d})}{\sqrt{\sum_{i=1}^{N} (Conc_{hi} - \overline{Conc_h})^2 \sum_{i=1}^{N} (Conc_{di} - \overline{Conc_d})^2}}$, where $\overline{Conc_h}$)and $\overline{Conc_d}$ are the average (across all sites and times) corrected $PM_{2.5}$ concentrations estimated from corrections h and d respectively.

(4) The temporal Pearson correlation coefficient (**Figure 8**): $R_T = \frac{\sum_{t=1}^{M} (Conc_{ht} - \overline{Conc_h}))(Conc_{dt} - \overline{Conc_d})}{\sqrt{\sum_{t=1}^{M} (Conc_{ht} - \overline{Conc_h}))^2 \sum_{i=1}^{N} (Conc_{dt} - \overline{Conc_d})^2}}$

We characterized the uncertainty in the 'corrected' $PM_{2.5}$ estimates at each site across the different models using two metrics: a normalized range (NR) (**Figure 9a**) and uncertainty, calculated from the 95% confidence interval (CI) assuming a t-statistical distribution (**Figure 9b**). NR for a given site represents the spread of $PM_{2.5}$ across the different correction approaches.

(5) $NR = \frac{1}{M}\sum_{t=1}^{M} \frac{max_{k\in K}\ C_{kt} - min_{k\in K}\ C_{kt}}{\overline{C_t}}$

C_{kt} is the $PM_{2.5}$ concentration at hour *t* from the *k*th model from the ensemble of *K* (which in this case is 89) correction approaches. $\overline{C_t}$ represents the ensemble mean across the *K* different products at hour *t*. *M* is the total number of hours in our sample for which we have $PM_{2.5}$ data for the site under consideration.

For our sample (*K* = 89), we assume the variations in $PM_{2.5}$ across multiple models follows the Student-t distribution with the mean being the ensemble average. The confidence interval (*CI*) for the ensemble mean at a given time *t* is:

(6) $CI_t = \overline{C_t} + t^* \frac{SD_t}{\sqrt{K}}$

Where $\overline{C_t}$ represents the ensemble mean at time *t*; *t** is the upper $\frac{(1-CI)}{2}$ critical value for the t-distribution with *K*-1 degrees of freedom. For *K*=89, *t** for the 95% double tailed confidence interval is 1.99. SD_t is the sample standard deviation at time *t*.

(7) $SD_t = \sqrt{\frac{\sum_{k=1}^{K} (C_{k,t} - \overline{C_t})^2}{K-1}}$

We define an overall estimate of uncertainty as follows:

(8) $uncertainty = \frac{1}{M} \sum_{t=1}^{M} t^* \frac{SD_t}{\overline{C_t}\sqrt{K}}$, which can also be expressed as

(8) $uncertainty = \frac{1}{M} \sum_{t=1}^{M} \frac{CI_t - \overline{C_t}}{\overline{C_t}}$

2.3.6 Evaluating the sensitivity of hotspot detection across the network of sensors to the calibration method

One of the key use-cases of low-cost sensors is hotspot detection. We report the labels of sites that are the most polluted using calibrated measurements from the 89 different models using hourly data (**Section 3.1.6**) We repeat this process for daily, weekly and monthly-averaged calibrated measurements. We ignore missing measurements from the network when calculating time averaged values for the different time periods considered. We report the mean number of sensors that are ranked 'most polluted' across the different correction functions for the different averaging periods (**Figure 10**). We do this to identify if the choice of the calibration model impacts the hotspot identified by the network (i.e. depending on the calibration model different sites show up as the most polluted).

2.3.7 Supplementary Analysis: Evaluating transferability of calibration models developed in different pollution regimes

We evaluated model performance for true/reference $PM_{2.5}$ concentrations > 30 µg/m^3 and ≤ 30 µg/m^3, as Nilson et al. (2022) has shown that calibration models can have different performances in different pollution regimes. We chose to use 30 µg/m^3 as the threshold, as these concentrations account for the greatest differences in health and air pollution avoidance behavior impacts (Nilson et al., 2022). Lower concentrations ($PM_{2.5}$ ≤ 30 µg/m^3) represent most measurements observed in our network; better performance at these levels will ensure better day-to-day functionality of the correction. High $PM_{2.5}$ (> 30 µg/m^3) concentrations in Denver typically occur during fires. Better performance of the calibration models in this regime will ensure that the LCS network can accurately capture pollution concentrations under smoky conditions. In order to compare errors observed in the two different concentration ranges, in addition to reporting R and RMSE of the calibration approaches, we also report the normalized RMSE (normalized by the mean of the true concentrations) (**Tables S3** and **S4**).

2.3.8 Supplementary Analysis: Evaluating transferability of calibration models developed across different time aggregation intervals

One of the key advantages of LCS is that they report high frequency (time scales shorter than an hour) measurements of pollution. As reference monitoring stations provide hourly or daily average pollution values, most often the calibration model is developed using hourly averaged data and then applied to the unaggregated, high-frequency LCS measurements. We applied the calibration models described in **Tables 2** and **3** developed using hourly-averaged co-located measurements on minute-level measurements from the co-located LCS described in **Table S1**. We evaluated the performance of the corrected high-frequency measurements against the 'true' measurements from the corresponding reference monitor using the metrics R and RMSE (**Tables S5** and **S6**).

3 Results

3.1 Evaluating the correction models at the co-location sites

3.1.1 Evaluating the representativeness of meteorological conditions at the co-location sites of the entire network

Temperature at the co-located sites across the entire period of the experiment (from Jan 1 – Sep 30, 2021) were similar to those at the rest of Love My Air network (**Figure 2a**). The sensor CS19 is the only one that recorded lower temperatures than those at any of the other sites. Relative humidity at the co-located sites (three of the four co-located sites have a median RH close to 50 % or higher) is higher than at the other sites in the network (7 of the 12 other sites have a median RH < 50%) (**Figure 2b**).

We also compared meteorological conditions during the development of corrections C3 (Jan 1 - Jan 14, 2021) and C4 (Jan 1 - Jan 14, 2021, and May 1 - May 14, 2021), to those measured during the duration of network operation (C3: **Figures S10** and **S11**; C4: **Figures S12** and **S13**). Unsurprisingly, temperatures at the co-located sites during the development of C4 were more representative of the network than C3, although they were on average lower (median temperatures ~ 10 - 17^{0}C) than the average temperatures experienced by the network (median temperatures ~ 5 - 23^{0}C). RH values at co-located sites during C3 and C4 tend to be higher than conditions experienced by some Love My Air sensors.

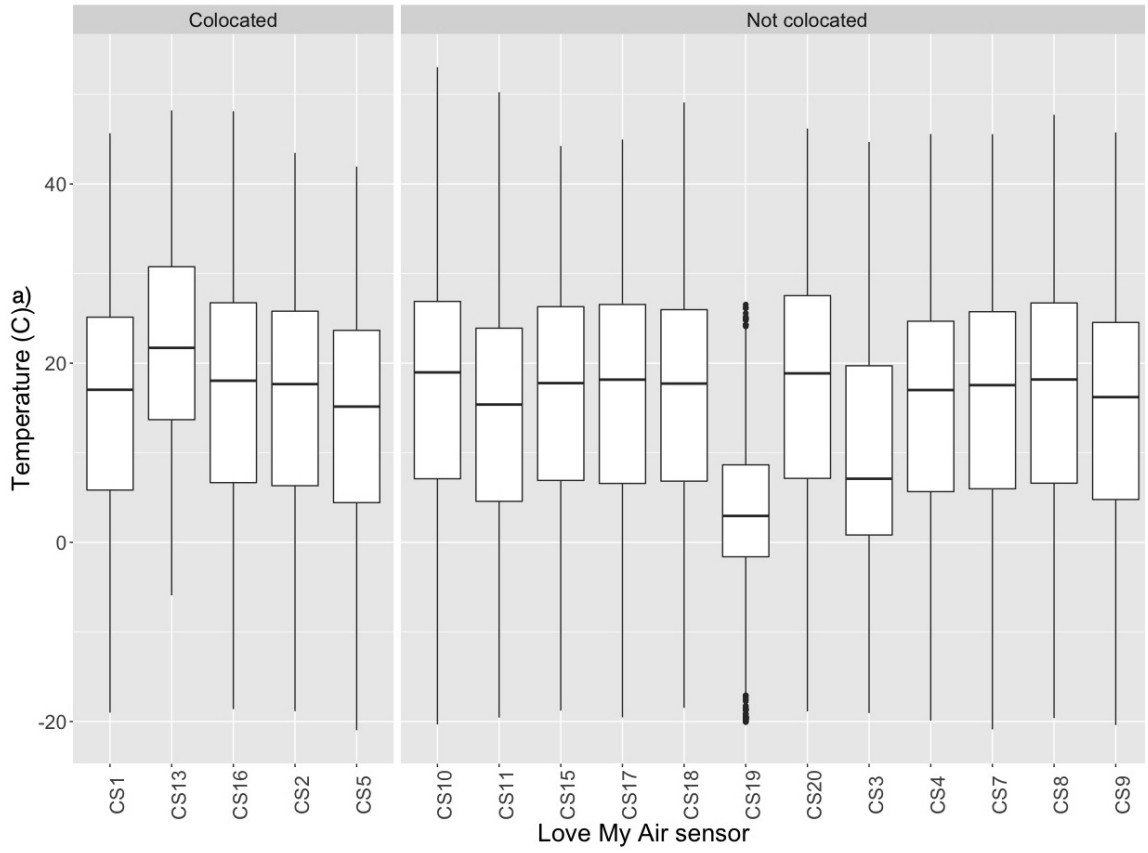
Colocated
Not colocated
a)
Temperature (C)
40
20
0
-20
CS1
CS13
CS16
CS2
CS5
CS10
CS11
CS15
CS17
CS18
CS19
CS20
CS3
CS4
CS7
CS8
CS9
Love My Air sensor

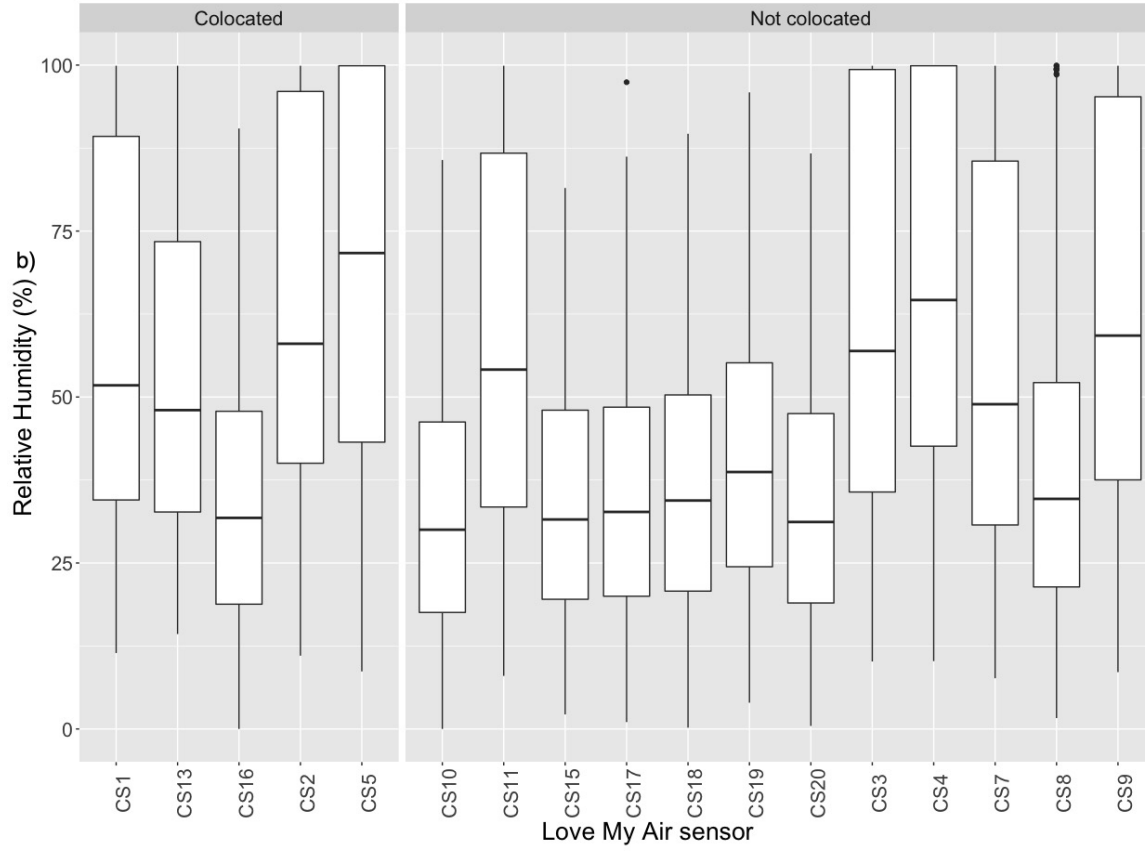
Colocated
Not colocated
b)
Relative Humidity (%)
100
75
50
25
0
CS1
CS13
CS16
CS2
CS5
CS10
CS11
CS15
CS17
CS18
CS19
CS20
CS3
CS4
CS7
CS8
CS9
Love My Air sensor

539

***Figure 2**: (a) Distribution of temperature recorded by each Love My Air sensor, (b) Distribution of RH recorded by each Love My Air sensor. The distribution of temperature and RH recorded by co-located LCS is shown on the left. The distribution of temperature and RH recorded by all LCS not used to construct the calibration models are displayed on the right*

3.1.2 Traditional Evaluation of the different Calibration Models

When we evaluated the performance of applying each of the 89 calibration models on all co-located data, we found that based on R and RMSE values, the on-the-fly C2 correction performed better overall than the C1, C3 and C4 corrections for most calibration model forms (**Tables 2** and **3**).

Within corrections C1 and C2, we found that an increase in complexity of model form resulted in a decreased RMSE. Overall, Model 21 yielded the best performance (RMSE = 1.281 μg/m^3 when using the C2 correction, 1.475 μg/m^3 when using the C1 correction with a LOSO CV and 1.480 μg/m^3 when using a LOBD correction). In comparison, the simplest model yielded an RMSE of 3.421 μg/m^3 for the C1 correction, and 3.008 μg/m^3 when using the C2 correction.

For correction C1, using a LOBD CV (**Table 3**) with the machine learning models resulted in better performance than using a LOSO CV (**Table 2**), except for Model 21 which is an RF model with additional time-of-day and month covariates, for which performance using the LOSO CV was marginally better (RMSE: 1.475 μg/m^3 versus 1.480 μg/m^3).

***Table 2**: Performance of the calibration models as captured using root mean square error (RMSE), and Pearson correlation (R). LOSO CV was used to prevent overfitting in the machine learning models. All corrected values were evaluated over the entire time-period (Jan 1 - Sep 30, 2021)*

ID	Name	Model	C1 *Correction developed on data during the entire period of network operation*	C2 *On-the-fly correction developed using data for the same week of measurement*	C3 *Correction developed using measurements made in the first two weeks of Jan*	C4 *Correction developed using measurements from the first two weeks of Jan and the first two weeks in May*

			R	RMSE ($\mu g/m^3$)	R	RMSE ($\mu g/m^3$)	R	RMSE ($\mu g/m^3$)	R	RMSE ($\mu g/m^3$)
	Raw Love My Air measurements									
0	Raw		0.927	6.469	-	-	-	-	-	-
	Multivariate Regression (LOSO CV)									
1	Linear	$PM_{2.5,\ corrected} = PM_{2.5} \times s1 + b$	0.927	3.421	0.944	3.008	0.927	3.486	0.927	3.424
2	+RH	$PM_{2.5,\ corrected} = PM_{2.5} \times s_1 + RH \times s_2 + b$	0.929	3.379	0.948	2.904	0.928	3.618	0.929	3.462
3	+T	$PM_{2.5,\ corrected} = PM_{2.5} \times s_1 + T \times s_2 + b$	0.928	3.409	0.949	2.896	0.925	3.948	0.928	3.460
4	+D	$PM_{2.5,\ corrected} = PM_{2.5} \times s_1 + D \times s_2 + b$	0.928	3.417	0.947	2.934	0.917	3.713	0.925	3.470
5	+RH x T	$PM_{2.5,\ corrected} = PM_{2.5} \times s_1 + RH \times s_2 + T \times s_3 + RH \times T \times s_4 + b$	0.934	3.260	0.953	2.782	0.931	3.452	0.933	3.344
6	+RH x D	$PM_{2.5,\ corrected} = PM_{2.5} \times s_1 + RH \times s_2 + D \times s_3 + RH \times D \times s_4 + b$	0.930	3.361	0.953	2.785	0.911	3.973	0.929	3.461
7	+D x T	$PM_{2.5,\ corrected} = PM_{2.5} \times s_1 + D \times s_2 + T \times s_3 + D \times T \times s_4 + b$	0.928	3.409	0.952	2.798	0.888	5.698	0.921	3.720
8	+RH x T x D	$PM_{2.5,\ corrected} = PM_{2.5} \times s_1 + RH \times s_2 + T \times s_3 + D \times s_4 + RH \times T \times s_5 + RH \times D \times s_6 + T \times D \times s_7 + RH \times T \times D \times s_8 + b$	0.935	3.246	0.955	2.724	0.779	7.077	0.926	3.625
9	PM x RH	$PM_{2.5,\ corrected} = PM_{2.5} \times s_1 + RH \times s_2 + RH \times PM_{2.5} \times s_3 + b$	0.930	3.362	0.950	2.854	0.925	3.949	0.925	3.767
10	PM x D	$PM_{2.5,\ corrected} = PM_{2.5} \times s_1 + D \times s_2 + D \times PM_{2.5} \times s_3$	0.932	3.324	0.950	2.871	0.883	4.460	0.913	3.777

		+ b								
11	PM x T	$PM_{2.5, corrected} = PM_{2.5} \times s_1 + T \times s_2 + T \times PM_{2.5} \times s_3 + b$	0.930	3.365	0.952	2.809	0.906	6.509	0.928	3.466
12	PM x nonlinear RH	$PM_{2.5, corrected} = PM_{2.5} \times s_1 + \frac{RH^2}{(1-RH)} \times s_2 + \frac{RH^2}{(1-RH)} \times PM_{2.5} \times s_3 + b$	0.934	3.277	0.948	2.900	0.931	3.510	0.932	3.403
13	PM x RH x T	$PM_{2.5, corrected} = PM_{2.5} \times s_1 + RH \times s_2 + T \times s_3 + PM_{2.5} \times RH \times s_4 + PM_{2.5} \times T \times s_5 + RH \times T \times s_6 + PM_{2.5} \times RH \times T \times s_7 + b$	0.938	3.165	0.956	2.672	0.891	6.220	0.928	3.497
14	PM x RH x D	$PM_{2.5, corrected} = PM_{2.5} \times s_1 + RH \times s_2 + D \times s_3 + PM_{2.5} \times RH \times s_4 + PM_{2.5} \times D \times s_5 + RH \times D \times s_6 + PM_{2.5} \times RH \times D \times s_7 + b$	0.933	3.288	0.957	2.663	0.879	7.289	0.917	4.033
15	PM x T x D	$PM_{2.5, corrected} = PM_{2.5} \times s_1 + T \times s_2 + D \times s_3 + PM_{2.5} \times T \times s_4 + PM_{2.5} \times D \times s_5 + T \times D \times s_6 + PM_{2.5} \times T \times D \times s_7 + b$	0.932	3.315	0.957	2.665	0.734	6.302	0.905	4.574
16	PM x RH x T x D	$PM_{2.5, corrected} = PM_{2.5} \times s_1 + RH \times s_2 + T \times s_3 + D \times s_4 + PM_{2.5} \times RH \times s_5 + PM_{2.5} \times T \times s_6 + T \times RH \times s_7 + PM_{2.5} \times D \times s_8 + D \times RH \times s_9 + D \times T \times s_{10} + PM_{2.5} \times RH \times T \times s_{11} + PM_{2.5} \times RH \times D \times s_{12} + PM_{2.5} \times D \times T \times s_{13} + D \times RH \times T \times s_{14} + PM_{2.5} \times RH \times T \times D \times s_{15} + b$	0.940	3.115	0.960	2.557	0.324	32.951	0.765	6.746
	Machine Learning (LOSO CV)									
17	Random Forest	$PM_{2.5, corrected} = f(PM_{2.5}, T, RH)$	0.983	1.713	0.988	1.450	0.913	3.926	0.911	3.824

18	Neural Network (One hidden layer)	$PM_{2.5,\ corrected}$ = f($PM_{2.5}$, T, RH)	0.933	3.286	0.948	2.916	0.932	3.550	0.913	4.725
19	Gradient Boosting	$PM_{2.5,\ corrected}$ = f($PM_{2.5}$, T, RH)	0.950	2.870	0.964	2.452	0.910	3.854	0.909	3.834
20	SuperLearner	$PM_{2.5,\ corrected}$ = f($PM_{2.5}$, T, RH)	0.950	2.855	0.970	2.236	0.910	3.917	0.923	3.582
21	Random Forest	For C1: $PM_{2.5,\ corrected}$ = f($PM_{2.5}$, T, RH, D, cos_time, cos_month, sin_month) For C2, C3, C4 $PM_{2.5,\ corrected}$ = f($PM_{2.5}$, T, RH, D, cos_time)	0.987	1.475	0.990	1.289	0.870	5.032	0.884	4.617

Table 3*: Performance of the calibration models using the C1 correction as captured using root mean square error (RMSE), and Pearson correlation (R) LOBD CV was used to prevent overfitting in the machine learning models*

ID	**Machine Learning (LOBD CV)**		**R**	**RMSE** ($\mu g/m^3$)
17	Random Forest	$PM_{2.5,\ corrected}$ = f($PM_{2.5}$, T, RH)	0.983	1.710
18	Neural Network (One hidden layer)	$PM_{2.5,\ corrected}$ = f($PM_{2.5}$, T, RH)	0.933	3.285
19	Gradient Boosting	$PM_{2.5,\ corrected}$ = f($PM_{2.5}$, T, RH)	0.953	2.759
20	SuperLearner	$PM_{2.5,\ corrected}$ = f($PM_{2.5}$, T, RH)	0.956	2.692
21	Random Forest	$PM_{2.5,\ corrected}$ = f($PM_{2.5}$, T, RH, D, cos_time, cos_month, sin_month)	0.987	1.480

3.1.3 Evaluating transferability of short-term calibrations developed to the entire period of operation of the network

We also found that for corrections of short-term calibrations, C3 and C4, more complex models yielded a better performance (for example the RMSE for Model 16: 2.813 $\mu g/m^3$, RMSE for Model 2: 3.110 $\mu g/m^3$ generated using the C3 correction) when evaluated

during the period of co-location, alone (**Table S3**). However, when models generated using the C3 and C4 corrections were transferred to the entire time period of co-location, we find that more complex multivariate regression models (Models 13-16) and the machine learning model (Model 21) that include cos_time, performed significantly worse than the simpler models (**Table 2**). In some cases, these models performed worse than the uncorrected measurements. For example, applying Model 16 generated using C3 on the entire dataset resulted in an RMSE of 32.951 μg/m^3 compared to 6.469 μg/m^3 for the uncorrected measurements.

Including data from another season, spring in addition to winter, in the training sample (C4), resulted in significantly increased performance of the calibration over the entire dataset compared to C3 (winter), although it did not result in an improvement in performance for all models compared to the uncorrected measurements. For example, Model 16 generated using C4 yielded an RMSE of 6.746 μg/m^3. Among the multivariate regression models, we found that models of the same form that corrected for RH instead of T or D did best. The best performance was observed for models that included the nonlinear correction for RH (Model 12) or included an $RH \times T$ term (Model 5) (**Table 2**).

3.1.4 Evaluating if the calibration models are overfitted to the co-location sites even after appropriate cross-validation

Figure 3 shows the performance (RMSE) of corrected Love My Air $PM_{2.5}$ data by generating corrections based on the 21 models previously proposed using the C1 correction, CV= LOSO and CV = LOBD for Models 17 - 21, when leaving out a test site (**Figure 3a**). Also shown is the result using the C1 correction when leaving out a three week period of data at a time and generating calibration models based on the data from the remaining time periods across each site, using CV = LOBD for Models 17 – 21, and applying the models to the remaining three-week period (**Figure 3b**). Finally, **Figures 3c, 3d** and **3e** illustrate using the C2, C3 and C4 corrections, respectively, (CV= LOSO for Models 17 - 21) when leaving out a test site.

Large reductions in RMSE are observed when applying simple linear corrections (Models 1 - 4) to the uncorrected data across C1, C2, C3 and C4. Increasing the complexity of the model does not result in marked changes in correction performance on different test sets for C1 and C2. Although the performance of the corrected datasets did improve on average for some of the complex models considered (Model 17, 20, 21 for example, vis-a-vis simple linear regressions when using the C1 correction) (**Figures 3a, 3b**), this was not the case for *all* test datasets considered, as evinced by the overlapping distributions of RMSE performances (e.g., Model 11 using the C2 correction resulted in a worse fit for one of the test datasets). For C3 and C4, the performance of corrections was worse across all datasets for the more complex multivariate model formulations (**Figures 3d**, **3e**), indicating that using uncorrected data is better than using these corrections and calibration models.

Wilcoxon tests and t-tests (based on whether Shapiro-Wilk tests revealed that the distribution of RMSEs was normal) revealed significant improvements in the distribution of RMSEs for all corrected test sets vis-a-vis the uncorrected data. There was no significant difference in the distribution of RMSE values from applying C1 and C2 corrections to the test sets, across the different models. For corrections C3 and C4, we found significant differences in the distribution of RMSEs obtained from running different models on the data, implying that the choice of model has a significant impact on transferability of the calibration models to other monitors.

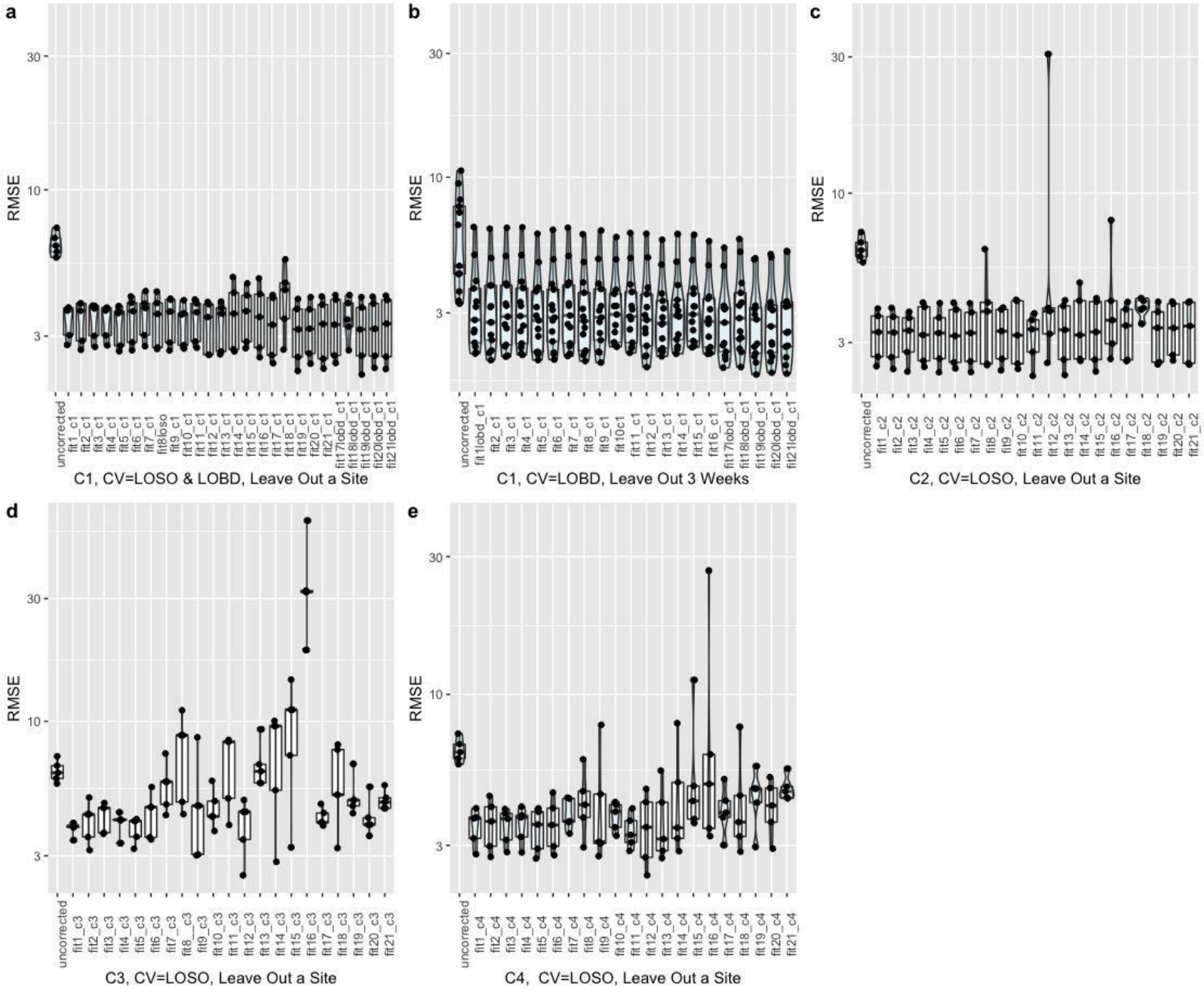

Figure 3*: Performance (RMSE) of corrected Love My Air $PM_{2.5}$ data by generating corrections based on the 21 models (designated as fit) previously proposed using* ***(a)*** *Correction C1 when leaving out a co-location site in turn and then running the generated correction on the test site (Note that for machine learning models (Models 17- 21), we*

*performed CV using a LOSO CV as well as a LOBD CV approach), **(b)** Correction C1 when leaving out 3 week periods of data at a time and generating corrections based on the data from the remaining time periods across each site, and evaluating the performance of the developed corrections on the held out 3 weeks of data (Note that for machine learning models (Models 17- 21), we performed CV using a LOBD CV approach), **(c)** Correction C2 when leaving out a co-location site in turn and then running the generated correction on the test site, **(d)** Correction C3 when leaving out a co-location site in turn and then running the generated correction on the test site, **(e)** Correction C4 when leaving out a co-location site in turn and then running the generated correction on the test site. Each point represents the RMSE for each test dataset permutation. The distribution of RMSEs is displayed using box-plots and violin-plots.*

The time-series of corrected $PM_{2.5}$ values for Models 1, 2, 5, 16, and 21 (RF using additional variables) (using CV = LOSO for the machine learning Models 17 and 21) for corrections generated using C1, C2, C3 and C4 are displayed in **Figure 4** for Love My Air sensor CS1. These subsets of models were chosen as they cover the range of model forms considered in this analysis.

From **Figure 4**, we note that although the different corrected values from C1 and C2 track each other well, there are small systematic differences between the different corrections. Peaks in corrected values using C2 tend to be higher than those using C1. Peaks in corrected values using machine learning methods using C1 are higher than those generated from multivariate regression models. **Figure 4** also shows marked differences in the corrected values from C3 and C4. Specifically Model 16 yields peaks in the data that corrections using the other models do not generate. This pattern was consistent when applying this suite of corrections to other Love My Air sensors.

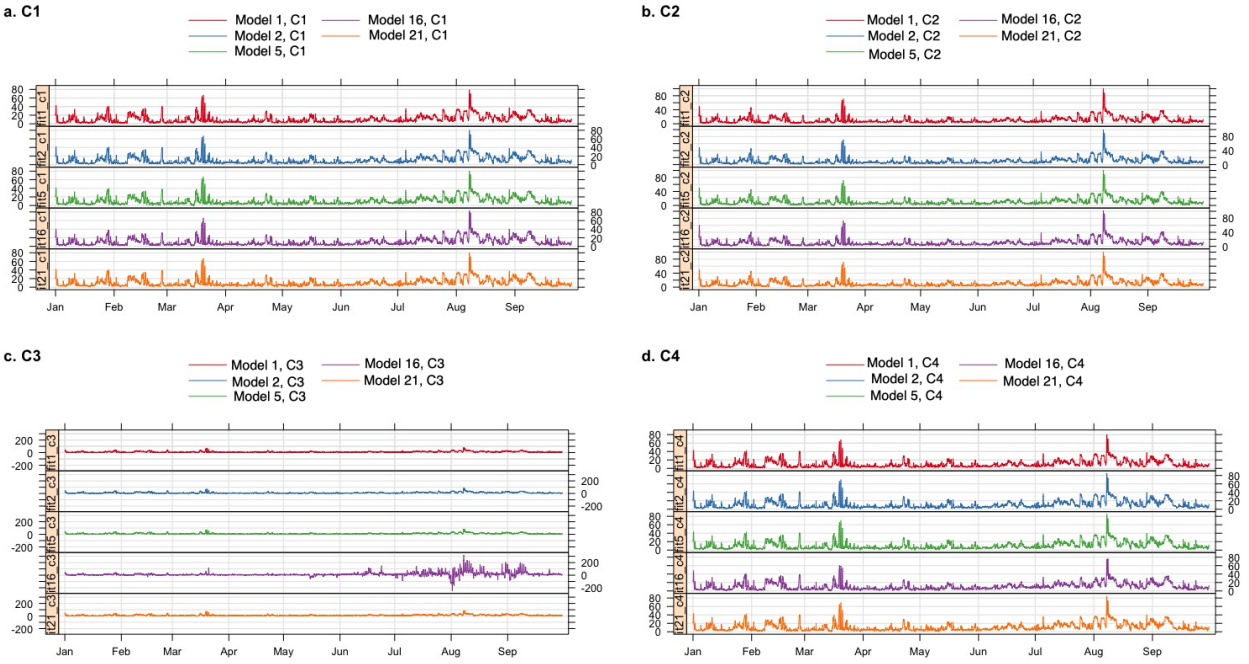

***Figure 4**: Time-series of the different $PM_{2.5}$ corrected values for Models 1, 2, 5, 16 and 21 across corrections (a) C1, (b) C2, (c) C3 and (d) C4 for the Love My Air monitor CS1. Note that the scales are the same for C1, C2 and C4, but not for C3.*

3.1.5 Evaluating sensitivity of the spatial and temporal trends of the low-cost sensor network to the method of calibration

The spatial and temporal RMSD values between corrected values generated from applying each of the 89 models using the four different correction approaches across all monitoring sites in the Love My Air network are displayed **Figures 5** and **6**, respectively. There is larger temporal variation (max 32.79 μg/m^3), in comparison to spatial variations displayed across corrections (max: 11.95 μg/m^3). Model 16 generated using the C3 correction has the greatest spatial and temporal RMSD in comparison with all other models. Models generated using the C3 and C4 corrections displayed the greatest spatial and temporal RMSD vis-a-vis C1 and C2.

Figures S14- **S17** display spatial RMSD values between all models corresponding to corrections C1-C4, respectively, to allow for a zoomed in view of the impact of the different model forms for the 4 corrections. Similarly, **Figures S18**- **S21** display temporal RMSD values between all models corresponding to corrections C1-C4, respectively. Across all models the temporal RMSD between models is greater than the spatial RMSD.

Spatial and temporal correlation coefficients between corrected measurements generated from applying all 89 models using the four different correction approaches across the entire network are displayed in **Figures 7** and **8**, respectively. The spatial correlations are lower than temporal correlations between corrected measurements.

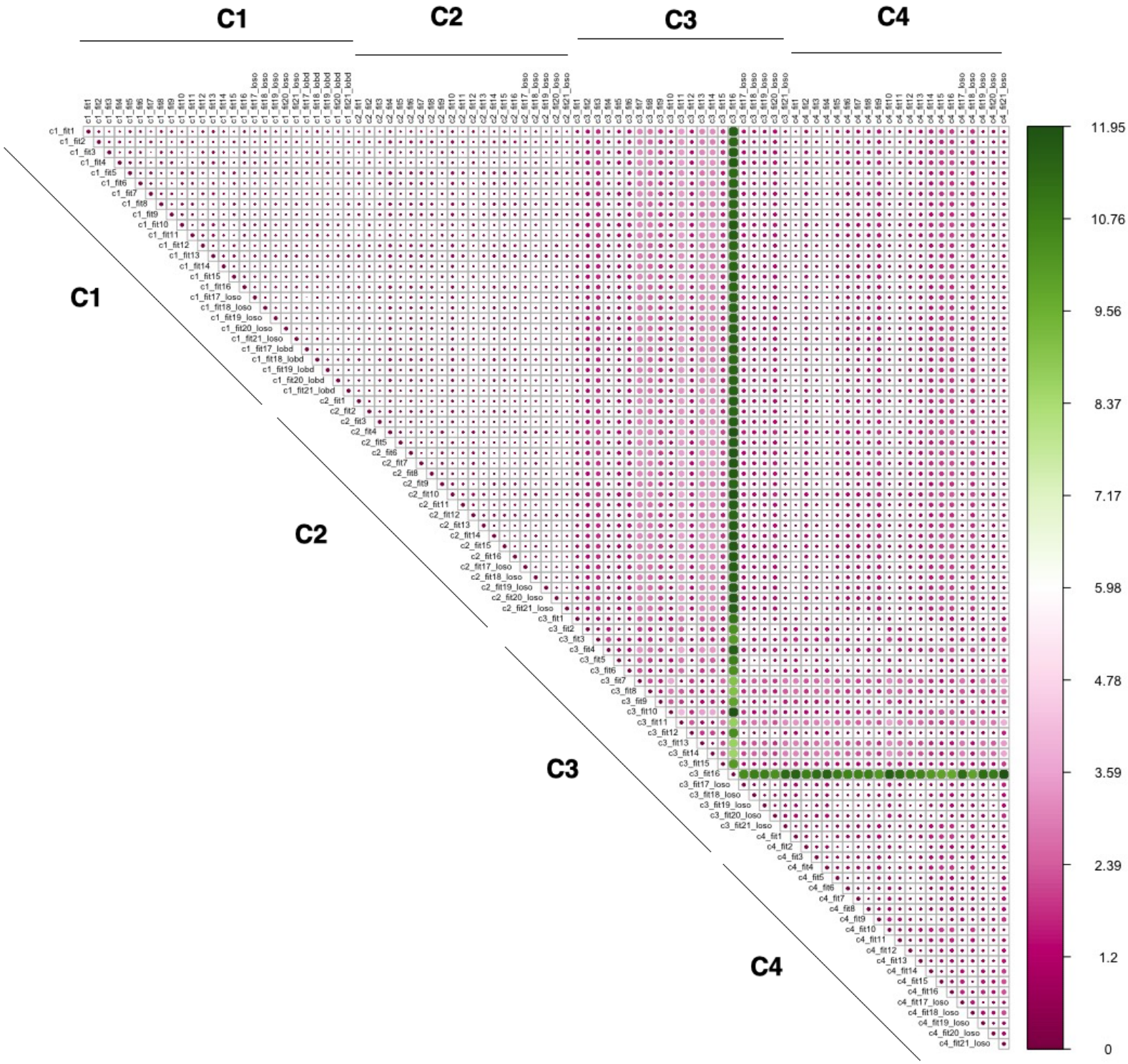

***Figure 5**: Spatial RMSD* (μg/m^3) *calculated using the method detailed in section 2.3.5 from applying each of the 89 calibration models using the four different correction approaches to all monitoring sites in the Love My Air network.*

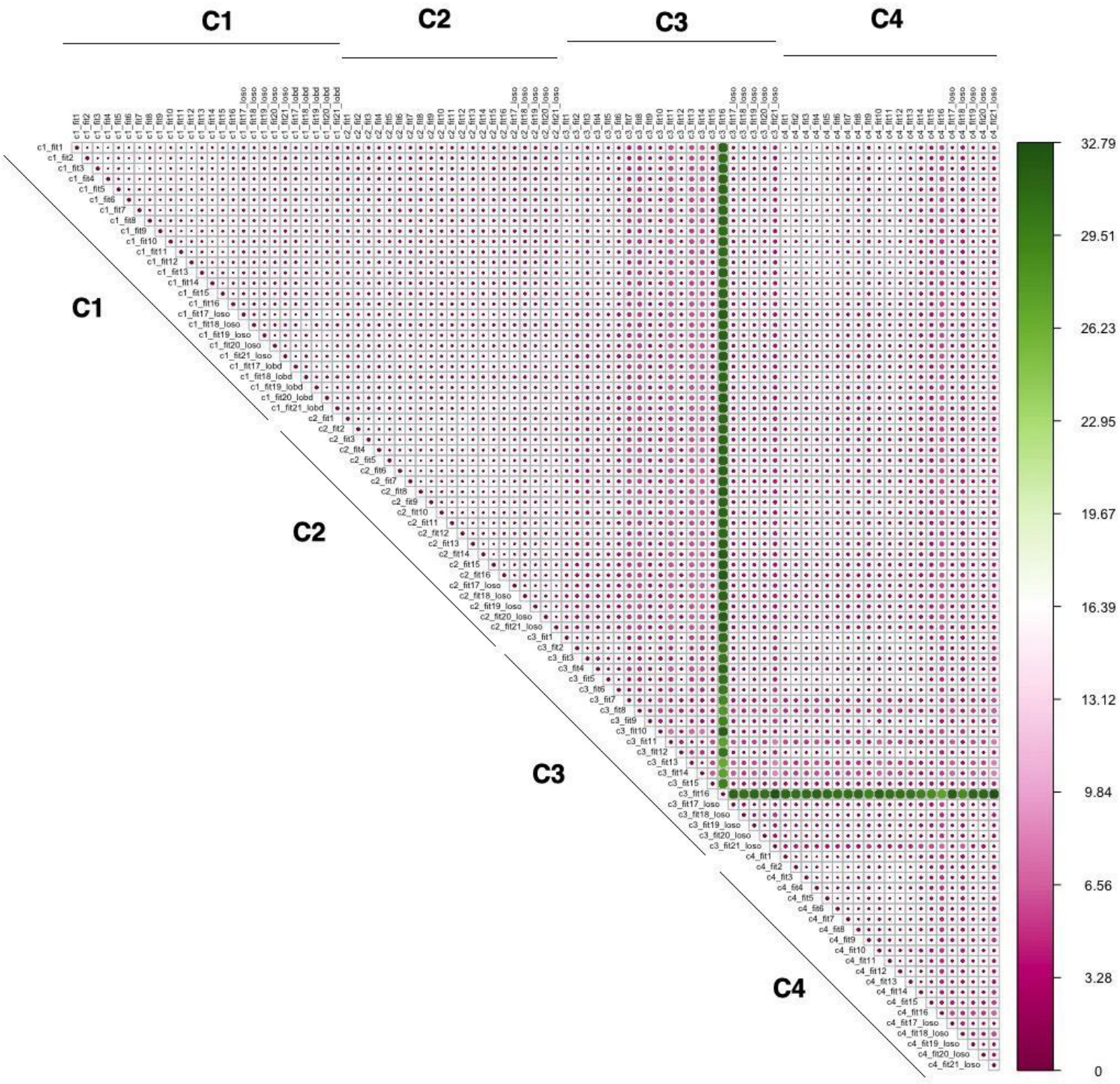

***Figure 6**: Temporal RMSD* (µg/m^3) *calculated using the method detailed in section 2.3.5 from applying each of the 89 calibration models using the four different correction approaches to all monitoring sites in the Love My Air network.*

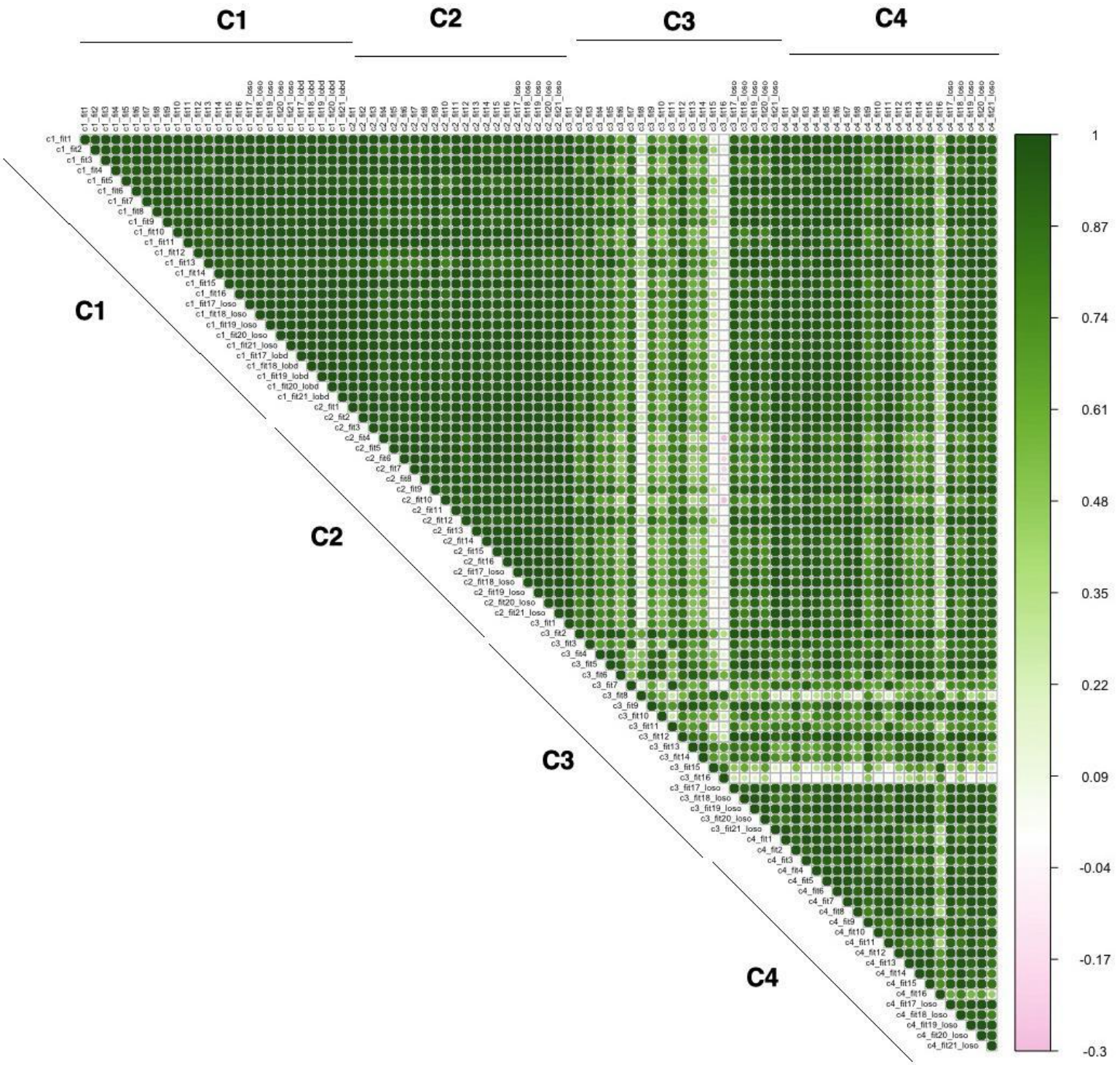

Figure 7: *Spatial Correlations from applying each of the 89 calibration models using corrections C1-C4 to all monitoring sites in the Love My Air network calculated using the method described in section 2.3.5.*

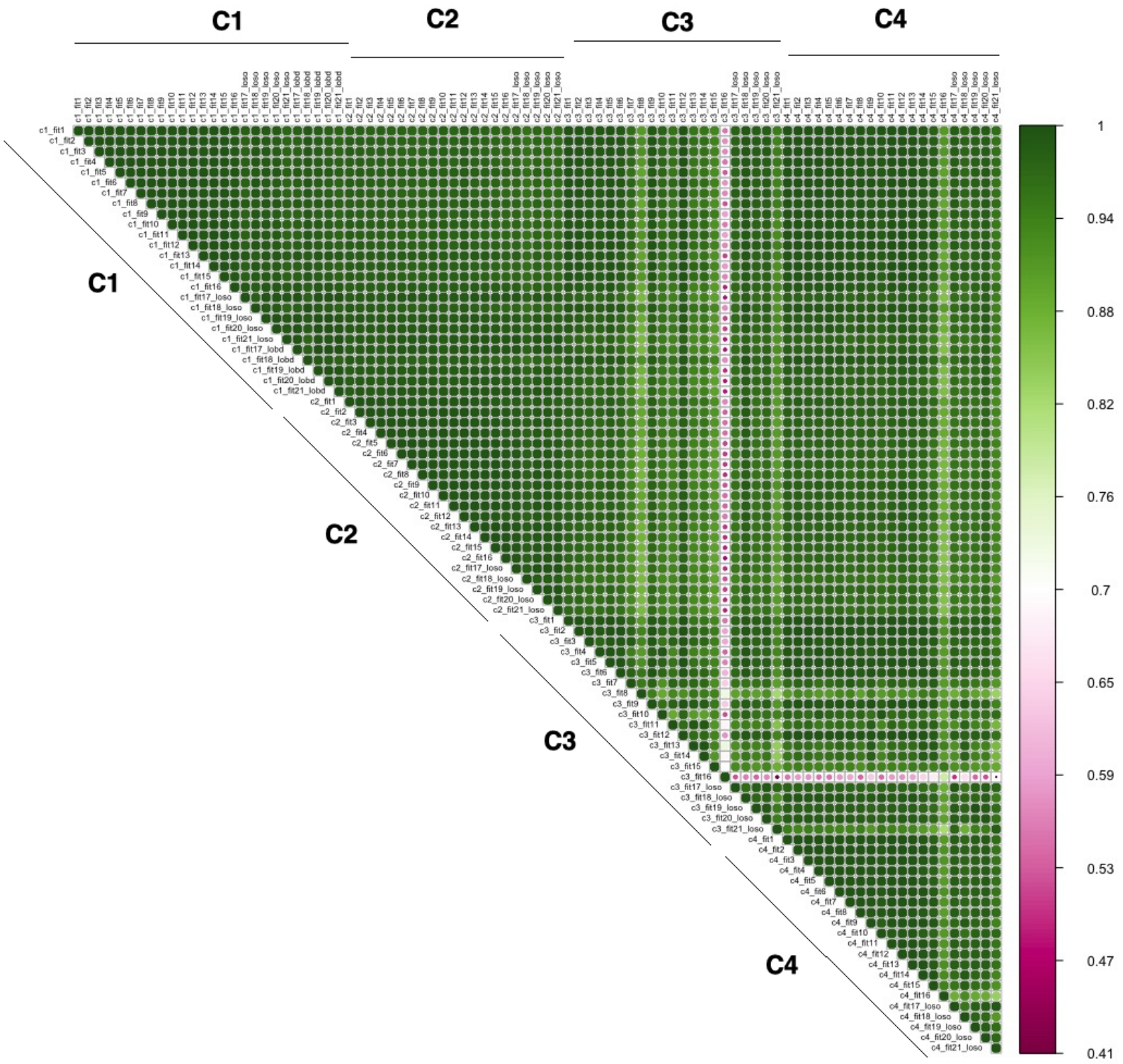

Figure 8: *Temporal Correlations from applying each of the 89 calibration models using corrections C1-C4 approaches to all monitoring sites in the Love My Air network calculated using the method described in section 2.3.5.*

The distribution of uncertainty and the NR in hourly-calibrated measurements over the 89 models by monitor are displayed in **Figure 9**. Overall, there are small differences in uncertainties and NR of the calibrated measurements across sites. The average NR and

uncertainty across all sites are 1.554 (median: 0.9768) and 0.044 (median: 0.033), respectively. We note that although the uncertainties in the data are small, the average normalized range tends to be quite large.

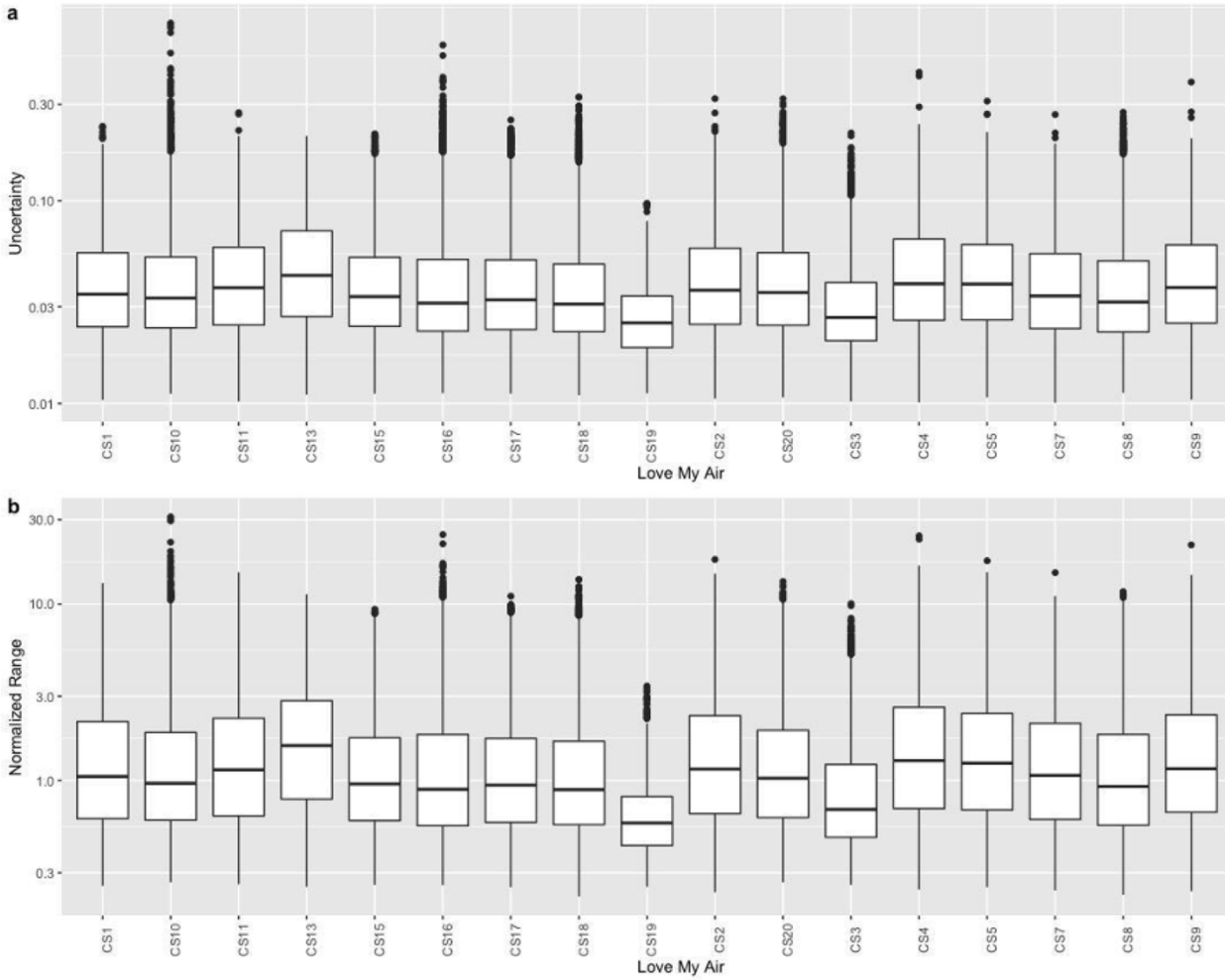

Figure 9*: Distribution of (a) uncertainty and (b) normalized range (NR) in hourly-calibrated measurements across all 89 calibration models at each site using the methodology described in Section 2.3.5.*

3.1.6 Evaluating the sensitivity of hotspot detection across the network of sensors to the calibration method

Mean (95% *CI*) $PM_{2.5}$ concentrations across the 89 different calibration models listed in **Tables 1** and **2**) at each Love My Air site for the duration of the experiment (Jan 1 - Sep 30, 2021) are displayed in **Figure S22**. Due to overlap between the different calibrated measurements across sites, the ranking of sites based on pollutant concentrations is dependent on the calibration model used.

Every hour, we ranked the different monitors for each of the 89 different calibration models, in order to evaluate how sensitive pollution hotspots were to the calibration model used. We found that there were on average 4.4 (median = 5) sensors that were ranked

most polluted. When this calculation was repeated using daily-averaged calibrated data, there were on average 2.5 (median = 2) sensors that were ranked the most polluted. The corresponding value for weekly-calibrated data was 2.4 (median = 1), and for monthly data was 3 (median = 3) (**Figure 9**).

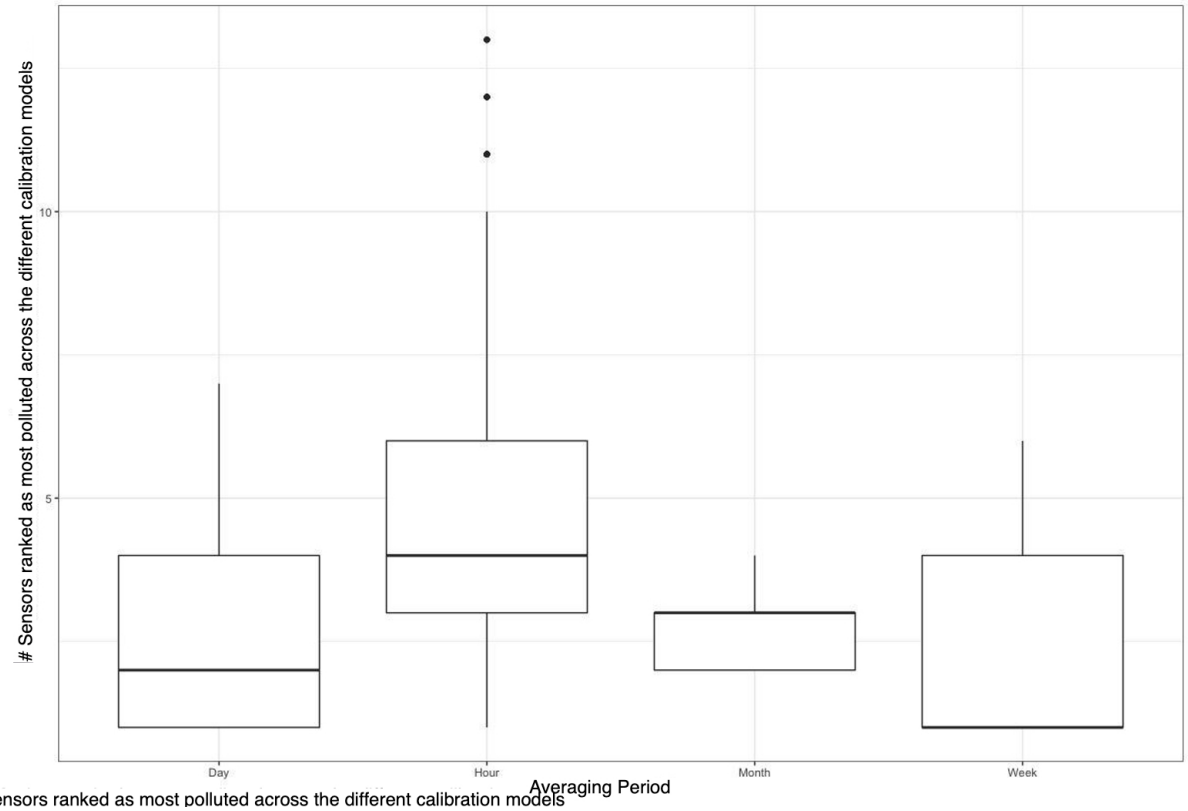

Sensors ranked as most polluted across the different calibration models

Figure 9: *Variation in the number of sites that were ranked as 'most polluted' across the 89 different calibration models for different time-averaging periods displayed using box-plots*

3.1.7 Supplementary Analysis: Evaluating transferability of calibration models developed in different pollution regimes

When we evaluated how well the models performed at high $PM_{2.5}$ concentrations (> 30 µg/m^3) versus lower concentrations (≤ 30 µg/m^3), we found that multivariate regression models generated using the C1 correction did not perform well in capturing peaks in $PM_{2.5}$ concentrations (normalized RMSE > 25%) (**Tables S3** and **S4**).

Multivariate regression models generated using the C2 correction performed better than those generated using C1 (normalized RMSE ~ 20 -25 %). Machine learning models generated using both C1 and C2 corrections captured $PM_{2.5}$ peaks well (C1: normalized RMSE ~ 10 - 25%, C2: normalized RMSE ~ 10 - 20%). Specifically, the C2 RF model (Model 21) yielded the lowest RMSE values (4.180 µg/m^3, normalized RMSE: 9.8%), of all models considered. The performance of models generated using C1 and C2 corrections in the low-concentration regime was the same as that over the entire dataset. This is because most measurements made were < 30 µg/m^3.

Models generated using C3 and C4 had the worst performance in both concentration regimes and yielded poorer agreement with reference measurements than even the uncorrected measurements. As in the case with the entire dataset, more complex multivariate regression models and machine learning models generated using C3 and C4 performed worse than more simple models in both $PM_{2.5}$ concentration intervals (**Tables S3** and **S4**).

3.1.8 Supplementary Analysis: Evaluating transferability of calibration models developed across different time aggregation intervals

We then evaluated how well the models generated using C1, C2, C3 and C4 corrections performed when applied to minute-level LCS data at co-located sites (**Tables S5** and **S6**). We found that the machine learning models generated using C1 and C2 improved the performance of the LCS. Model 21 (CV=LOSO) generated using C1 yielded an RMSE of 15.482 $\mu g/m^3$ compared to 16.409 $\mu g/m^3$ obtained from the uncorrected measurements.

The more complex multivariate regression models yielded a significantly worse performance across all corrections. (Model 16 generated using C1 yielded an RMSE of 41.795 $\mu g/m^3$). As in the case with the hourly-averaged measurements, using correction C1, LOBD CV instead of LOSO for the machine learning models resulted in better model performance except for Model 21. Few models generated using C3 and C4 resulted in improved performance when applied to the minute-level measurements (**Tables S5** and **S6**).

4 Discussion and Conclusions

In our analysis of how transferable the correction models developed at the Love My Air co-location sites are to the rest of the network, we found that for C1 and C2, more complex model forms yielded better predictions (higher R, lower RMSE) at the co-located sites. This is likely because the machine learning models were likely best able to capture complex, non-linear relationships between the LCS measurements, meteorological parameters and reference data. Model 21, which included additional covariates intended to capture periodicities in the data, such as seasonality yielded the best performance, suggesting that in this study the relationship between LCS measurements and reference data varies over time. One possible reason for this could be the impact of changing aerosol composition in time which has been shown to impact the LCS calibration function (Malings et al., 2020).

When examining the short-term, C3 and C4 corrections, we found that although these corrections appeared to significantly improve LCS measurements during the time period of model development (**Table S2**), when transferred to the entire time period of operation they did not perform well (**Table 2**). Many of the models, especially the more complex multivariate regression models, performed significantly worse than even the uncorrected measurements. This indicates that calibration models generated during short time

periods, even if the time periods correspond to different seasons, may not necessarily transfer well to other times, likely due to changes in the aerosol composition, and differences in meteorological conditions, among other potential factors. This indicates the need for statistical calibration models to be developed over longer time periods that better capture different LCS operating conditions. For C3 and C4, we did however find models that relied on nonlinear formulations of RH, that serve as proxies for hygroscopic growth, yielded the best performance, as compared to more complex models (**Table 2**). This suggests that physics-based calibrations are potentially an alternative approach, especially when relying on short co-location periods and need to be explored further.

When evaluating how transferable different calibration models were to the rest of the network, we found that for C1 and C2, more complex models that appeared to perform well at the co-location sites did not necessarily transfer best to the rest of the network. Specifically, when we tested these models on a co-located site that was left out when generating the calibration models, we found that some of the more complex models using the C2 correction yielded a significantly worse performance at some test sites (**Figure 3**). If the corrected data were going to be used to make site-specific decisions then such corrections would lead to important errors. For C3 and C4, we observed a large distribution of RMSE values across sites. For several of the more complex models developed using C3 and C4 corrections, the RMSE values at some left-out sites were larger than observed for the uncorrected data, suggesting that certain calibration models could result in even more error-prone data than using uncorrected measurements. As the meteorological parameters for the duration of the C3 and C4 co-locations are not representative of overall operating conditions of the network, it is likely that the more complex models were overfit to conditions during the co-location, leading to them not performing well over the network operations.

For C1 and C2, we found that there were no significant differences in the distribution of the performance metric RMSE of corrected measurements from simpler models in comparison to those derived from more complex corrections at test sites (**Figure 3**). For C3 and C4, we found significant differences in the distribution of RMSE across test sites, which indicates that these models are likely site-specific and not easily transferable to other sites in the network. This suggests that less complex models might be preferred when short-term co-locations are carried out for sensor calibration, especially when conditions during the short-term co-location are not representative of that of the network.

We found that the temporal RMSD (**Figure 6**) was greater than the spatial RMSD (**Figure 5**) for the ensemble of corrected measurements developed by applying the 89 different calibration models to the Love My Air network. One of the reasons this may be the case is that $PM_{2.5}$ concentrations across the different Love My Air sites in Denver are highly correlated (**Figure S5**), indicating that the contribution of local sources to $PM_{2.5}$ concentrations in the Denver neighborhoods in which Love My Air was deployed is small. Due to the low variability in $PM_{2.5}$ concentrations across sites, it makes sense that the

variations in the corrected $PM_{2.5}$ concentrations will be seen in time rather than space. The largest pairwise temporal RMSD were all seen between corrections derived from complex models using the C3 correction.

However, we note that the temporal correlation coefficients (**Figure 8**) for all-pairwise correction models was higher than the corresponding spatial coefficient (**Figure 7**). This implies that although the corrections generated from all models considered tended to track each other (except for a few models using C3) some corrected values were biased low, whereas some were biased high. It's important for future work to be done to characterize under what conditions these biases occur.

Finally, we observed that the uncertainty in $PM_{2.5}$ concentrations across the ensemble of 89 calibration models (**Figure 9**) was consistently small for the Love My Air Denver network. The normalized range in the corrected measurements, on the other hand, was large; however, the uncertainty (95% CI) in the corrected measurements fall within a relatively small interval. Thus, deciding which calibration model to pick has important consequences for decision-makers when using data from this network.

Our findings reinforce the idea that evaluating calibration models at all co-location sites using overall metrics like RMSE should not be seen as the only/best way to determine how to calibrate a network of LCS. Instead, approaches like the ones we have demonstrate, and metrics like the ones we have proposed should be used to evaluate calibration transferability.

We found that the detection of the 'most polluted' site in the Love My Air network (an important use-case of LCS networks) was dependent on the calibration model used on the network. We also found that for the Love My Air network, the detection of the most polluted site was sensitive to the duration of time-averaging of the corrected measurements (**Figure 10**). Hotspot detection was most robust using weekly-averaged measurements. A possible reason for this is that temporal variation in $PM_{2.5}$ in Denver varied primarily on a weekly-scale, and therefore analysis conducted using weekly-values resulted in the most robust results. Such an analysis thus provides guidance on the most useful temporal scale for decision-making related to evaluating hotspots in the Denver network.

In supplementary analyses, when we evaluated the sensitivity of other LCS use-cases to the calibration model applied such as tracking high pollution concentrations during fire or smoke-events, we found that different models yielded different performance results in different pollution regimens. Machine learning models developed using C1, and models developed using C2 were better than multivariate regression models generated using C1 at capturing peaks in pollution (> 30 $\mu g/m^3$). All models using C3 and C4 yielded poor performance results in tracking high pollution events (**Tables S3** and **S4**). This is likely because $PM_{2.5}$ concentrations during the C3 and C4 co-location tended to be low. The

calibration model developed thus did not transfer well to other concentrations. When evaluating how well the calibration models developed using hourly-aggregated measurements translated to high-resolution minute-level data (**Tables S5**and **S6**), we observed that machine learning models generated using C1 and C2, improved the LCS measurements. More complex multivariate regression models performed poorly. All C3 and C4 models also performed poorly. This suggests that caution needs to be exercised when transferring models developed at a particular time scale to another. Note that in this paper, because pollution concentrations did not show much spatial variation, we focus on evaluating transferability across time-scales, only.

In summary, this paper makes the case that it is not enough to evaluate calibration models based on metrics of performance at co-located sites, alone. We need to:

1) *Determine how well calibration adjustments can be transferred to other locations.* Specifically, although we found that in Denver some calibration models performed well at co-location sites, the models could result in large errors at specific sites that would create difficulties for site-specific decision making.

2) Examine how well calibration adjustments can be transferred to other time periods. In this study we found that models developed using the short-term C3 and C4 corrections were not transferable to other time periods because the conditions during the co-location were not representative of broader operating conditions in the network.

3) *Use a variety of approaches to quantify transferability of calibration models in the overall network* (e.g., with spatio-temporal correlations and RMSD). The metrics proposed in this paper to evaluate model transferability can be used in other networks.

4) *Investigate how adopting a certain time-scale for averaging measurements could mitigate the uncertainty induced by the calibration process for specific use-cases.* Namely, we found that in the Love My Air network, hotspot identification was more robust to using daily-averaged data than hourly-averaged data. Our analyses also revealed which models performed best when needing to transfer the calibration model developed using hourly-averaged data to higher-resolution data, and which models best captured peaks in pollution during fire- or smoke- events.

In this work, the Love My Air network under consideration is located over a fairly small area in a single city. In this network, for the time period considered, $PM_{2.5}$ seems to be mainly a regional pollutant and the contribution of local sources is small. More work needs to be done to evaluate model transferability in networks in other settings. Concerns about model transferability are likely to be even more pressing when thinking about larger networks that span different cities and should be considered in future research. In this study, we present a first attempt to demonstrate the importance of considering the

transferability of calibration models. In future work, we also aim to explore the physical factors that drive concerns about transferability to generalize our findings more broadly.

Author Contributions

PD conceptualized the study, developed the methodology, carried out the analysis and wrote the first draft. PD and BC obtained funding for this study. BC produced Figure 1. All authors helped in refining the methodology and editing the draft.

Acknowledgements

PD and BC gratefully acknowledge a CU Denver Presidential Initiative grant that supported their work. The authors are grateful to the Love My Air team for setting up and maintaining the Love My Air network. The authors are also grateful to Carl Malings for useful comments

Competing Interests

The authors declare that they have no conflict of interest.

References

Anderson, G. and Peng, R.: weathermetrics: Functions to convert between weather metrics (R package), 2012.

State of Global Air: https://www.stateofglobalair.org/, last access: 18 June 2022.

Apte, J. S., Messier, K. P., Gani, S., Brauer, M., Kirchstetter, T. W., Lunden, M. M., Marshall, J. D., Portier, C. J., Vermeulen, R. C. H., and Hamburg, S. P.: High-Resolution Air Pollution Mapping with Google Street View Cars: Exploiting Big Data, Environ. Sci. Technol., 51, 6999–7008, https://doi.org/10.1021/acs.est.7b00891, 2017.

Barkjohn, K. K., Gantt, B., and Clements, A. L.: Development and application of a United States-wide correction for $PM_{2.5}$ data collected with the PurpleAir sensor, Atmospheric Meas. Tech., 14, 4617–4637, https://doi.org/10.5194/amt-14-4617-2021, 2021.

Bean, J. K.: Evaluation methods for low-cost particulate matter sensors, Atmospheric Meas. Tech., 14, 7369–7379, https://doi.org/10.5194/amt-14-7369-2021, 2021.

Bi, J., Wildani, A., Chang, H. H., and Liu, Y.: Incorporating Low-Cost Sensor Measurements into High-Resolution PM2.5 Modeling at a Large Spatial Scale, Environ. Sci. Technol., 54, 2152–2162, https://doi.org/10.1021/acs.est.9b06046, 2020.

Brantley, H. L., Hagler, G. S. W., Herndon, S. C., Massoli, P., Bergin, M. H., and Russell, A. G.: Characterization of Spatial Air Pollution Patterns Near a Large Railyard Area in Atlanta, Georgia, Int. J. Environ. Res. Public. Health, 16, 535, https://doi.org/10.3390/ijerph16040535, 2019.

Castell, N., Dauge, F. R., Schneider, P., Vogt, M., Lerner, U., Fishbain, B., Broday, D., and

Bartonova, A.: Can commercial low-cost sensor platforms contribute to air quality monitoring and exposure estimates?, Environ. Int., 99, 293–302, https://doi.org/10.1016/j.envint.2016.12.007, 2017.

Clements, A. L., Griswold, W. G., Rs, A., Johnston, J. E., Herting, M. M., Thorson, J., Collier-Oxandale, A., and Hannigan, M.: Low-Cost Air Quality Monitoring Tools: From Research to Practice (A Workshop Summary), Sensors, 17, 2478, https://doi.org/10.3390/s17112478, 2017.

Considine, E. M., Reid, C. E., Ogletree, M. R., and Dye, T.: Improving accuracy of air pollution exposure measurements: Statistical correction of a municipal low-cost airborne particulate matter sensor network, Environ. Pollut., 268, 115833, https://doi.org/10.1016/j.envpol.2020.115833, 2021.

Crawford, B., Hagan, D.H., Grossman, I., Cole, E., Holland, L., Heald, C.L. and Kroll, J.H., 2021. Mapping pollution exposure and chemistry during an extreme air quality event (the 2018 Kīlauea eruption) using a low-cost sensor network. Proceedings of the National Academy of Sciences, 118(27), p.e2025540118.

Crilley, L. R., Shaw, M., Pound, R., Kramer, L. J., Price, R., Young, S., Lewis, A. C., and Pope, F. D.: Evaluation of a low-cost optical particle counter (Alphasense OPC-N2) for ambient air monitoring, Atmospheric Meas. Tech., 11, 709–720, https://doi.org/10.5194/amt-11-709-2018, 2018.

deSouza, P. and Kinney, P. L.: On the distribution of low-cost PM 2.5 sensors in the US: demographic and air quality associations, J. Expo. Sci. Environ. Epidemiol., 31, 514–524, https://doi.org/10.1038/s41370-021-00328-2, 2021.

deSouza, P., Anjomshoaa, A., Duarte, F., Kahn, R., Kumar, P., and Ratti, C.: Air quality monitoring using mobile low-cost sensors mounted on trash-trucks: Methods development and lessons learned, Sustain. Cities Soc., 60, 102239, https://doi.org/10.1016/j.scs.2020.102239, 2020a.

deSouza, P., Lu, R., Kinney, P., and Zheng, S.: Exposures to multiple air pollutants while commuting: Evidence from Zhengzhou, China, Atmos. Environ., 118168, https://doi.org/10.1016/j.atmosenv.2020.118168, 2020b.

deSouza, P. N.: Key Concerns and Drivers of Low-Cost Air Quality Sensor Use, Sustainability, 14, 584, https://doi.org/10.3390/su14010584, 2022.

deSouza, P. N., Dey, S., Mwenda, K. M., Kim, R., Subramanian, S. V., and Kinney, P. L.: Robust relationship between ambient air pollution and infant mortality in India, Sci. Total Environ., 815, 152755, https://doi.org/10.1016/j.scitotenv.2021.152755, 2022.

Giordano, M. R., Malings, C., Pandis, S. N., Presto, A. A., McNeill, V. F., Westervelt, D. M., Beekmann, M., and Subramanian, R.: From low-cost sensors to high-quality data: A summary of challenges and best practices for effectively calibrating low-cost particulate matter mass sensors, J. Aerosol Sci., 158, 105833, https://doi.org/10.1016/j.jaerosci.2021.105833, 2021.

Hagler, G. S. W., Williams, R., Papapostolou, V., and Polidori, A.: Air Quality Sensors and Data Adjustment Algorithms: When Is It No Longer a Measurement?, Environ. Sci. Technol., 52, 5530–5531, https://doi.org/10.1021/acs.est.8b01826, 2018.

Holstius, D. M., Pillarisetti, A., Smith, K. R., and Seto, E.: Field calibrations of a low-cost aerosol sensor at a regulatory monitoring site in California, Atmospheric Meas. Tech., 7, 1121–1131, https://doi.org/10.5194/amt-7-1121-2014, 2014.

Jin, X., Fiore, A. M., Civerolo, K., Bi, J., Liu, Y., Donkelaar, A. van, Martin, R. V., Al-Hamdan, M., Zhang, Y., Insaf, T. Z., Kioumourtzoglou, M.-A., He, M. Z., and Kinney, P. L.: Comparison of multiple PM 2.5 exposure products for estimating health benefits of emission controls over New York State, USA, Environ. Res. Lett., 14, 084023, https://doi.org/10.1088/1748-9326/ab2dcb, 2019.

Johnson, N. E., Bonczak, B., and Kontokosta, C. E.: Using a gradient boosting model to improve the performance of low-cost aerosol monitors in a dense, heterogeneous urban environment, Atmos. Environ., 184, 9–16, https://doi.org/10.1016/j.atmosenv.2018.04.019, 2018.

Kim, K.-H., Kabir, E., and Kabir, S.: A review on the human health impact of airborne particulate matter, Environ. Int., 74, 136–143, https://doi.org/10.1016/j.envint.2014.10.005, 2015.

Kuhn, M.: caret: Classification and Regression Training, Astrophys. Source Code Libr., ascl:1505.003, 2015.

Kumar, P., Morawska, L., Martani, C., Biskos, G., Neophytou, M., Di Sabatino, S., Bell, M., Norford, L., and Britter, R.: The rise of low-cost sensing for managing air pollution in cities, Environ. Int., 75, 199–205, https://doi.org/10.1016/j.envint.2014.11.019, 2015.

Liang, L.: Calibrating low-cost sensors for ambient air monitoring: Techniques, trends, and challenges, Environ. Res., 197, 111163, https://doi.org/10.1016/j.envres.2021.111163, 2021.

Magi, B. I., Cupini, C., Francis, J., Green, M., and Hauser, C.: Evaluation of PM2.5 measured in an urban setting using a low-cost optical particle counter and a Federal Equivalent Method Beta Attenuation Monitor, Aerosol Sci. Technol., 54, 147–159, https://doi.org/10.1080/02786826.2019.1619915, 2020.

Malings, C., Tanzer, R., Hauryliuk, A., Saha, P. K., Robinson, A. L., Presto, A. A., and Subramanian, R.: Fine particle mass monitoring with low-cost sensors: Corrections and long-term performance evaluation, Aerosol Sci. Technol., 54, 160–174, https://doi.org/10.1080/02786826.2019.1623863, 2020.

Morawska, L., Thai, P. K., Liu, X., Asumadu-Sakyi, A., Ayoko, G., Bartonova, A., Bedini, A., Chai, F., Christensen, B., Dunbabin, M., Gao, J., Hagler, G. S. W., Jayaratne, R., Kumar, P., Lau, A. K. H., Louie, P. K. K., Mazaheri, M., Ning, Z., Motta, N., Mullins, B., Rahman, M. M., Ristovski, Z., Shafiei, M., Tjondronegoro, D., Westerdahl, D., and Williams, R.: Applications of low-cost sensing technologies for air quality monitoring and exposure assessment: How far have they gone?,

Environ. Int., 116, 286–299, https://doi.org/10.1016/j.envint.2018.04.018, 2018.

Nilson, B., Jackson, P. L., Schiller, C. L., and Parsons, M. T.: Development and Evaluation of Correction Models for a Low-Cost Fine Particulate Matter Monitor, Atmospheric Meas. Tech. Discuss., 1–16, https://doi.org/10.5194/amt-2021-425, 2022.

Singh, A., Ng'ang'a, D., Gatari, M. J., Kidane, A. W., Alemu, Z. A., Derrick, N., Webster, M. J., Bartington, S. E., Thomas, G. N., Avis, W., and Pope, F. D.: Air quality assessment in three East African cities using calibrated low-cost sensors with a focus on road-based hotspots, Environ. Res. Commun., 3, 075007, https://doi.org/10.1088/2515-7620/ac0e0a, 2021.

Snyder, E. G., Watkins, T. H., Solomon, P. A., Thoma, E. D., Williams, R. W., Hagler, G. S. W., Shelow, D., Hindin, D. A., Kilaru, V. J., and Preuss, P. W.: The Changing Paradigm of Air Pollution Monitoring, Environ. Sci. Technol., 47, 11369–11377, https://doi.org/10.1021/es4022602, 2013.

Spinelle, L., Gerboles, M., Villani, M. G., Aleixandre, M., and Bonavitacola, F.: Calibration of a cluster of low-cost sensors for the measurement of air pollution in ambient air, in: 2014 IEEE SENSORS, 2014 IEEE SENSORS, 21–24, https://doi.org/10.1109/ICSENS.2014.6984922, 2014.

Van der Laan, M. J., Polley, E. C., and Hubbard, A. E.: Super learner, Stat. Appl. Genet. Mol. Biol., 6, 2007.

West, S. E., Buker, P., Ashmore, M., Njoroge, G., Welden, N., Muhoza, C., Osano, P., Makau, J., Njoroge, P., and Apondo, W.: Particulate matter pollution in an informal settlement in Nairobi: Using citizen science to make the invisible visible, Appl. Geogr., 114, 102133, https://doi.org/10.1016/j.apgeog.2019.102133, 2020.

Williams, R., Kilaru, V., Snyder, E., Kaufman, A., Dye, T., Rutter, A., Russel, A., and Hafner, H.: Air Sensor Guidebook, US Environmental Protection Agency, Washington, DC, EPA/600/R-14/159 (NTIS PB2015-100610), 2014.

Zimmerman, N., Presto, A. A., Kumar, S. P. N., Gu, J., Hauryliuk, A., Robinson, E. S., Robinson, A. L., and R. Subramanian: A machine learning calibration model using random forests to improve sensor performance for lower-cost air quality monitoring, Atmospheric Meas. Tech., 11, 291–313, https://doi.org/10.5194/amt-11-291-2018, 2018.

Zusman, M., Schumacher, C. S., Gassett, A. J., Spalt, E. W., Austin, E., Larson, T. V., Carvlin, G., Seto, E., Kaufman, J. D., and Sheppard, L.: Calibration of low-cost particulate matter sensors: Model development for a multi-city epidemiological study, Environ. Int., 134, 105329, https://doi.org/10.1016/j.envint.2019.105329, 2020.